U.S. DEPARTMENT OF COMMERCE
NATIONAL OCEANIC AND ATMOSPHERIC ADMINISTRATION
NATIONAL WEATHER SERVICE
NATIONAL METEOROLOGICAL CENTER

OFFICE NOTE 249

An Efficient and Effective Explicit Damping Time Integration Scheme

Clifford H. Dey
Development Division

DECEMBER 1981

This is an unreviewed manuscript, primarily intended for informal exchange of information among NMC staff members.

An Efficient and Effective Explicit Damping Time Integration Scheme

by Clifford Dey

I. Introduction

There are two general classes of solutions permitted by the set of primitive equations we use to describe atmospheric motions -- meteorological modes and gravity-inertia modes. The meteorological modes most closely describe the atmospheric motions that produce most of our everyday weather and are therefore the ones we seek to predict. Gravity-inertia motions, although present in the atmosphere, are generally of much less importance. In numerical prediction models, however, the amplitudes of the gravity-inertia modes can become abnormally large and interfere with the prediction of the more important synoptic-scale meteorological motions. One method of dealing with this problem has been to develop time integration schemes that reduce the amplitudes of the gravity-inertia motions while leaving the meteorological motions relatively untouched.

There are two general types of selectively damping time integration schemes. One type are those whose damping is frequency-dependent. They rely on the fact that many of the most offensive gravity-inertia motions have much higher frequencies than do the meteorological modes in order to achieve their selectivity. Examples of frequency-dependent damping integration schemes are the Euler-backward method (Matsuno, 1966) and the Robert time filter (Robert, 1966). The second type of damping time integration schemes achieve their selectivity by treating the linear terms of the model equations, which are most closely associated with gravity-inertia motion, differently from the nonlinear advection terms. The best-known scheme of this type is the semi-implicit backward method

(Kurihara, 1965). The only explicit technique in this class is a variation of the Euler-backward scheme described by Kurihara and Tripoli (1976).

All of the explicit damping time integration schemes require more computer time than the nondamping methods. This seems a rather high price to pay for noise control. In this paper, an explicit, selectively damping time integration scheme is described that requires substantially less computer time than simple centered differences. The computational economy is achieved by incorporating into the centered time integration method a damping procedure originally conceived by Okamura (see Nitta, 1969) and later generalized by Grant (1974). The next section describes the basic concept of incorporating the generalized Okamura technique into the centered time difference scheme. The integration method itself, the Semi-Interative Method, is presented and analysed in Section III. Simple numerical tests of the Semi-Iterative Method are described in the fourth section. Section V contains some concluding remarks.

II. Application of the generalized Okamura procedure to centered differences in time

The basic idea behind the semi-iterative method, which will be discussed in the next section, is to incorporate the generalized Okamura technique into the centered difference time integration scheme in a particular way. Before considering the semi-iterative scheme in its entirety, however, it will be instructive to consider the effects of introducing the generalized Okamura technique into centered time differences with a simple example.

Consider the oscillation equation

$$\frac{\partial \phi}{\partial t} = -ikc\phi , \tag{1}$$

where ϕ is any variable, t is time, k the wave number, and c is

the phase speed. A centered difference representation of this equation is

(2) $$\phi^{\tau+1} = \phi^{\tau-1} - 2ia\phi^{\tau} ,$$

where $a = kc\Delta t$, Δt is the time step, and $\tau\Delta t$ is the time level. The generalized Okamura technique applied to ϕ^{τ} is represented by the equations

(3) $$\begin{aligned} \hat{\phi} &= \phi^{\tau} - ia\phi^{\tau} , \\ \hat{\hat{\phi}} &= \hat{\phi} + ia\phi^{\tau} , \\ \tilde{\phi}^{\tau} &= (1+\alpha)\phi^{\tau} - \alpha\hat{\hat{\phi}} . \end{aligned}$$

Elimination of reference to $\hat{\hat{\phi}}$ in (3) gives

(4) $$\tilde{\phi}^{\tau} = (1 - \alpha a^2)\phi^{\tau} .$$

α can be positive number. The first way of incorporating this potent damping device into (2) is to replace ϕ^{τ} with its damped counterpart, $\tilde{\phi}^{\tau}$. Using (4) one then obtains

(5) $$\phi^{\tau+1} = \phi^{\tau-1} - i2aB\phi^{\tau} ,$$

in which $B = 1-\alpha a^2$ (note that this can be done n times. Then $B = (1-\alpha a^2)^n$. In this note, only n=1 will be considered).

In order to analyze the effect of this substitution, let ϕ^{τ} be represented by

$$\phi^{\tau} = \phi_0 \xi^{\tau} .$$

Let ξ^{τ}, the time-dependent part of ϕ^{τ}, be given by

$$\xi^{\tau} = e^{-ikc^*\tau\Delta t} ,$$

where c* is the numerical phase velocity. Thus,

$$\begin{aligned} \xi^{\tau+1} &= \lambda\xi^{\tau} , \\ \xi^{\tau-1} &= \lambda^{-1}\xi^{\tau} . \end{aligned}$$

where $\lambda = e^{-ikc^*\Delta t}$. Furthermore,

(6) $$\begin{aligned} \phi^{\tau+1} &= \lambda\phi^{\tau} , \\ \phi^{\tau-1} &= \lambda^{-1}\phi^{\tau} . \end{aligned}$$

In general, λ is a complex number $(\lambda = \lambda_r + i\lambda_i)$. The magnitude of the time-dependent part of the solution is

(7) $$|\lambda| = \{\lambda_r^2 + \lambda_i^2\}^{1/2} ,$$

while the numerical phase angle (θ) is given by

$$\theta = \tan^{-1}\left\{\frac{\lambda_i}{\lambda_r}\right\} .$$

However, it will be more convenient to refer to the ratio (R) of the numerical to the analytic (-a) phase angle. R is given by

(8) $$R = -\frac{1}{a}\tan^{-1}\left\{\frac{\lambda_i}{\lambda_r}\right\} .$$

Substituting (6) into (5), multiplying through by λ, and rearranging terms results in

(9) $$\lambda^2 + i2aB\lambda - 1 = 0 .$$

The roots of (9) are given by

(10) $$\lambda = -iaB \pm \{-a^2B^2 + 1\}^{1/2} .$$

When $-a^2B^2 + 1 < 0$, at least one root of (9) will always be unstable. However, when $-a^2B^2 + 1 \geq 0$, the magnitude of both roots is unity. Recalling the definition of B, the stability requirement becomes

$$-a^2(1 - \alpha a^2)^2 + 1 \geq 0 .$$

considering the equality and expanding in terms of α, one finds

(11) $$a^4\alpha^2 - 2a^2\alpha + 1 - 1/a^2 = 0 .$$

The two solutions for α in (11) are:

(12) $$\alpha_+ = \frac{1}{a^2}\left\{1 + \frac{1}{a}\right\} ; \quad \alpha_- = \frac{1}{a^2}\left\{1 - \frac{1}{a}\right\} .$$

Graphs of α_+ and α_- are given in Fig. 1. The α_- root reaches a maximum somewhere around a=3/2, then decreases. The α_+ root, on the other hand, decreases monotonically, reaching the maximum value of α_- around a=3. To fix these values with more assurance, note that

$$\frac{\partial\alpha_-}{\partial a} = -\frac{2}{a^3} + \frac{3}{a^4} .$$

Since $\partial\alpha_-/\partial a$ is zero when a=3/2, the maximum value of α_- is indeed reached at that point. From (12), $\alpha_- = 4/27$ when a=3/2. Since, also from 12), $\alpha_+ = 4/27$ when a=3, the maximum time step in this case is three times as long as the usual centered difference time step. Everywhere in the stable region, the amplitude response is neutral. Graphs of $|\lambda|$ and R are given as a function of a for α = 4/27 in Figs. 2 and 3, respectively.

Another way to incorporate the genralized Okamura technique into centered time differences is to replace $\phi^{\tau-1}$ with its damped counterpart. Then, (2) becomes

(13) $$\phi^{\tau+1} = B\phi^{\tau-1} - 2ia\phi^{\tau},$$

where, as before, $B = 1 - \alpha a^2$. Proceeding as in the previous case, (13) becomes

(14) $$\lambda^2 + 2ia\lambda - B = 0$$

The roots of (14) are

(15) $$\lambda = -ia \pm \{-a^2 + B\}^{1/2}$$

Here, stability will always occur for $-a^2 + B \geq 0$. Then,

(16) $$|\lambda| = \{1 - \alpha a^2\}^{1/2}$$

The magnitude can be made less than 1 for any value of a by an appropriate choice of α. The question is for what values of a will the inequality hold. Utilizing the definition of B, the inequality can be written as

$$-a^2 + 1 - \alpha a^2 \geq 0$$

or

(17) $$\alpha \leq \frac{1}{a^2} - 1$$

Since α must be positive, the maximum value of a for which (17) will hold is 1. As α increases, damping increases but the maximum allowable value of a decreases. The region for which $-a^2 + B \geq 0$ is shown in Fig. 4.

However, the scheme is not always unstable when $-a^2+B<0$. In the narrow strip between the solid and dashed lines in Fig. 4, the scheme is stable even though $-a^2+B<0$. Graphs of $|\lambda|$ and R are given as a function of a for $\alpha=1.0$ in Figs. 5 and 6, respectively.

The third way of incorporating the generalized Okamura technique into centered time differences is to replace both ϕ^{τ} and $\phi^{\tau-1}$ with their damped counterparts. Here, (2) becomes

(18) $$\phi^{\tau+1} = B\phi^{\tau-1} - i2aB\phi^{\tau},$$

where B is defined as before. Proceeding as in the previous cases, (18) becomes

(19) $$\lambda^2 + i2aB\lambda - B = 0 .$$

The roots of (19) are

(20) $$\lambda = -iaB \pm \{-a^2B^2 + B\}^{1/2} .$$

In this case, stability always occurrs for $-a^2B^2+B\geq 0$. Then, the magnitude of both roots is given by

$$|\lambda| = \{1-\alpha a^2\}^{1/2},$$

which is the same as in the previous case. Once again, the question is for what values of a will the inequality hold. Recalling the definition of B, the requirement becomes

$$-a^2(1-\alpha a^2)^2 + (1-\alpha a^2) \geq 0$$

Proceeding as with the first case, consider now the equality and expand in terms of α. Then,

(21) $$a^6\alpha^2 + (a^2-2a^4)\alpha + (a^2-1) = 0$$

The two solutions for α in (21) are

(22) $$\alpha_+ = \frac{1}{a^2} \; ; \; \alpha_- = \frac{1}{a^2}\left\{1-\frac{1}{a^2}\right\} .$$

Graphs of α_+ and α_- are given in Figure 7. (As in Fig. 4, in the narrow strip between the solid and dashed lines, the scheme is stable even though

$-a^2B^2+B<0$.). Note the similarity between Figs. 7 and 1. In contrast with the first case, however, this scheme is a damping one everywhere within the stable region. In order to determine the maximum allowable time step, note that

$$\frac{\partial \alpha_-}{\partial a} = -\frac{2}{a^3} + \frac{4}{a^5} .$$

The maximum value of α_- occurrs for $a=\sqrt{2}$, at which point $\alpha_-=\frac{1}{4}$. The value of a for $\alpha_+=\frac{1}{4}$ is 2, or twice that of the usual centered difference formulation (actually because of the stable region for $-a^2B^2+B<0$, the maximum value of a when $\alpha=\frac{1}{4}$ is nearly 2.2). Graphs of $|\lambda|$ and R are given as a function of a for $\alpha=\frac{1}{4}$ in Figs. 8 and 9, respectively.

To summarize the results of this section, there are three basic ways of incorporating the generalized Okamura technique into a centered time difference scheme. If the technique is applied only to the $\tau\Delta t$ time level, the time step may be increased by up to a factor of three, but no damping results. If the technique is applied only to the $(\tau-1)\Delta t$ time level, strong damping results, but the maximum allowable time step is reduced. If the scheme is applied to both the $\tau\Delta t$ and $(\tau-1)\Delta t$ time levels, on the other hand, the maximum allowable time step is increased by over a factor of 2 yet strong damping is still achieved. In the latter two cases, the amount of damping may be selected by varying the parameter α.

Although each of these three choices results in a scheme with interesting characteristics, none is very practical. First, all the tendency terms must be computed an extra two times for each iteration of the generalized Okamura technique. Second, the damping is frequency-dependent and therefore not very selective. Third, an extra set of fields is required. In each case, however, the generalized Okamura technique can be applied to centered

time differences in such a way that the first two objections are removed. The result, referred to as the semi-iterative scheme, features both computational efficiency and highly selective damping. The next section describes and analyzes the semi-iterative scheme and suggests that it is a very attractive alternative to existing explicit time integration schemes.

III. The Semi-Iterative Method

In order to illustrate the semi-iterative method, consider the following system of linear equations:

(23) $$\frac{\partial u}{\partial t} + \bar{u}\frac{\partial u}{\partial x} - fv + g\frac{\partial h}{\partial x} = 0 ,$$

(24) $$\frac{\partial v}{\partial t} + \bar{u}\frac{\partial v}{\partial x} + fu = 0 ,$$

(25) $$\frac{\partial h}{\partial t} + \bar{u}\frac{\partial h}{\partial x} - \frac{f\bar{u}}{g} + \bar{h}\frac{\partial u}{\partial x} = 0 ,$$

in which $\bar{u}$ is a constant zonal current, $\bar{h}$ is the mean depth of the fluid varying only in the y direction such that

(26) $$\bar{u} = -\frac{g}{f}\frac{\partial \bar{h}}{\partial y} ,$$

and u,v, and h are pertubation wind components and height, respectively.

Assume the solutions to (23)-(25) are of the form

(27) $$\begin{bmatrix} u \\ v \\ h \end{bmatrix} = \begin{bmatrix} u_o \\ v_o \\ h_o \end{bmatrix} e^{ik(x-ct)} ,$$

where c is the phase speed, k is the wave number ($k = \frac{2\pi}{L}$, L=wavelength), and u_o, v_o, and h_o are unknown amplitudes. Substitution of (27) into (23)-(25) and requiring the determinant of the resulting system of linear equations to vanish produces an equation for the phase speed c;

(28) $$(\bar{u}-c)^3 - \left(g\bar{h} + \frac{f^2}{k^2}\right)(\bar{u}-c) + \frac{f^2}{k^2}\bar{u} = 0 .$$

There are three real roots of (28), given by

(29) $$c_1 = \bar{u} + 2\sqrt{-a/3}\,\cos\left[\theta/3\right]$$

(30) $$c_2 = \bar{u} + 2\sqrt{-a/3}\,\cos\left[\theta/3 + 2\pi/3\right]$$

(31) $$c_3 = \bar{u} + 2\sqrt{-a/3}\,\cos\left[\theta/3 + 4\pi/3\right]$$

where

(32) $$a = -\left[g\bar{h} + \frac{f^2}{k^2}\right], \quad b = \frac{f^2}{k^2}\bar{u}, \quad \text{and } \theta = \cos^{-1}\left[-\frac{b}{2}\left[-\frac{a^3}{27}\right]^{-1/2}\right]$$

C_1, C_2, and C_3 denote the phase velocity of a meteorological wave, an eastward moving external gravity-inertia wave, and a westword moving external gravity-inertia wave, respectively.

Referring to C_1, C_2, and C_3 as C_j, j=1,3 and expressing u_o and v_o in terms of h_o, the solutions to (25) may be written as

(33) $$u = \sum_{j=1}^{3} u_j, \quad u_j = \phi_j \frac{k^2(\bar{u}-c)}{f^2-k^2(\bar{u}-c_j)^2},$$

(34) $$v = \sum_{j=1}^{3} v_j, \quad v_j = \phi_j \frac{ikf}{f^2-k^2(\bar{u}-c_j)^2},$$

(35) $$\phi = \sum_{j=1}^{3} \phi_j, \quad \phi_j = \phi_{o_j} e^{ik(x-ct)}.$$

It can be shown (Kurihara, 1965, op. cit) that with substitution of (33)-(35) into the original system, any one of (23)-(25) can be written in the form

(36) $$\frac{\partial h_j}{\partial t} + ik\bar{u}h_j + ik(c_j-\bar{u})h_j = 0, \quad h = \sum_{j=1}^{3} h_j,$$

where h_j represents u_j,v_j, or $_j$. This fact allows the analysis of the semi-iterative method to proceed by considering only one equation of the form of (27) rather than to the original system of three equations.

Using centered differences in time, equation (36) may be written as

$$h_j^{\tau+1} = h_j^{\tau-1} - 2ik\bar{u}\Delta t\, h_j^{\tau} - 2ik(c_j-\bar{u})\Delta t\, h_j^{\tau},$$

or letting $a = k\bar{u}\Delta t$ and $b = k(c_j-\bar{u})\Delta t$, as

(37) $$h_j^{\tau+1} = h_j^{\tau-1} - 2i(a+b)h_j^{\tau}.$$

The semi-iterative method consists of applying the generalized Okamura technique to the terms associated with gravitational oscillations (those

involving b), then using the resulting damped fields for the tendency calculations and/or to step from when making a centered time step. In this case, the generalized Okamura technique applied to the fields at the time level is written as

$$\hat{h}_j = h_j^{\tau} - ib\,h_j^{\tau} ,$$

$$\tilde{h}_j = \hat{h}_j + ib\,\hat{h}_j ,$$

$$\tilde{h}_j^{\tau} = (\alpha+1)h_j^{\tau} - \alpha h_j^{\tau} = (1-\alpha b^2)h_j^{\tau} .$$

If this proces is iterated n times, then one finds

(38) $$\tilde{h}_j^{\tau} = (1-\alpha b^2)^n h_j^{\tau} .$$

where it is entirely permissible for α to be different (but always positive) on each iteration. In a similar manner, m generalized Okamura iterations on the $\tau-1$ fields results in

(39) $$\tilde{h}_j^{\tau-1} = (1-\beta b^2)^m h_j^{\tau-1}$$

Once again, β may differ on each iteration. Replacing h_j^{τ} and $h_j^{\tau-1}$ in (37) by their damped counterparts given by (38) and (39) produces the semi-iterative method. The result is

(40) $$h_j^{\tau+1} = (1-\beta b^2)^m h_j^{\tau-1} - 2i(a+b)(1-\alpha b^2)^n h_j^{\tau}$$

The analysis of (40) proceeds as in the previous section. Thus (40) becomes

(41) $$\lambda^2 + 2i(a+b)(1-\alpha b^2)^n\lambda - (1-\beta b^2)^m = 0$$

However, rather than evaluating the roots of (41) as in the previous section, a computer program was used. There are many combinations of α, β, m, and n that could be examined. By way of example two categories of combinations will be described in this section. They are:

Category 1: m=1, α = 0.0, 0.1, 0.2, 0.3, 0.4, 0.5, n=0, β=0.

Category 2: m=n-1, $\alpha=\beta$= 0.0, 0.1, 0.2, 0.3, 0.4, 0.5.

Category 1 is one iteration of the generalized Okamura procedure applied only to h_j^{τ}, using six different values of α (when α =0

in category 1, the system reduces to simple centered differences in time). Using the results of the previous section as a guide, we would expect this to provide an increased time step but no damping. Category 2 is one generalized Okamura iteration applied to both h_j^{τ} and $h_j^{\tau-1}$ using six different values for α and β (when $\alpha=\beta=0$ in category 2, the system reduces to simple centered differences in time). By setting $\alpha=\beta$, a separate iteration of the generalized Okamura procedure would not need to be performed on the $\tau-1$ fields in actual practice. Again using the previous section as a guide, we might expect the combinations in this category to result in an increased time step (although less than in category 1) and strong damping. As before, the effect of finite differences in space is not considered in this simple analysis. In all the graphs shown in this section, both the amplitude of λ and the ratio of the numerical to the analytical phase speed are given as functions of a ($a=kc\Delta t$) where the wave length is assumed to be 2000 km.

The six category 1 configurations are described in Figures 10-15. The behavior of the meteorological mode is shown in Figures 10 and 11. The most important thing to note here is that the graphs are the same for all values of α. The effect of the semi-iterative method for category 1 configurations is thus restricted to the gravity-inertia modes, which are described in figures 12-15.

The gravity-inertia modes are shown for various values of α, with a mean geopotential of 8×10^4 m^2s^{-2} in figures 12 and 13. Note there is no damping in the stable region for any choice of α. When α =0.1, a large unstable region appears at a=1.0 and continues to a=3.1. Then there is another stable region that extends to a=4.1. However, little or no

increase in the time step is allowed until the intermediate instability area is eliminated. As α increases, the unstable region separating the two stable regions shrinks, and the limit (in terms of a) on the second stable region shrinks as well. By the time α =0.3, the intermediate unstable region disappears, and the stability limit is at a=2.5. The comparison to the results of Section II can be seen by recalling Figure 1. There, the α curve rose above zero for a $\geq$1.0. This is the same (intermediate) unstable region that can be seen in Figure 12. In both figures, the intermediate unstable area was avoided by making α sufficiently large. Figure 13 shows that when α=0.3, the gravity-inertia wave phase speed is reduced for all values of a below the stability limit. The graphs terminate when the physical and computational mode curves meet, for the computer program is unable to distinguish one from the other thereafter. This should be of little importance, however, because this point is very close to the stability limit.

Figures 14 and 15 describe the effect of reducing the mean geopotential while holding α fixed at 0.25. At first, as the mean geopotential is reduced, the stability limit increases. However, by the time $\overline{\Phi}$ becomes $2\times10^{4}\,m^{2}s^{-2}$, the intermediate instability area noted in Figure 12 appears, substantially reducing the maximum allowable time step. The intermediate instability area for small values of $\overline{\Phi}$ can be eliminated by increasing α. We note from Figure 12 that this reduces the maximum allowable time step somewhat. In effect, the maximum allowable time step for this use of the semi-iterative method will be determined by the internal gravity-inertia modes, for they will require the largest values of α to eliminate the intermediate instability area. As expected, there is no damping when the semi-interative method is applied only to the τ fields.

The behavior of six category 2 configurations are described in Figures 16-21. The meteorological modes are shown in Figures 16 and 17. There is no effect on the meteorolgical modes when the semi-iterative method is applied to both the τ and τ-1 fields. One of the goals of this use of the semi-iterative method has therefore been attained-there is neither damping nor phase speed changes of the meteorological modes.

Figures 18 and 19 describe the behavior of the gravity-inertia modes for various values of α, where $\overline{\Phi}$ is held constant at 8×10^4 m^2s^{-2}. In this case, there is strong damping of the gravity-inertia modes throughout the stable regions. These graphs are similar to those in Figure 12 in that the intermediate instability area is once again present. It is eliminated when α and β are ≥ 0.4 (not the actual minimum value needed). When α and $\beta = 0.4$, very strong damping of the gravity-inertia modes occurrs for $a \leq 1.86$. Thereafter, the computational mode quickly becomes unstable while the physical mode continues to be damped. Therefore, the other two goals of this use of the semi-iterative method are also achieved - strong damping of the gravity-inertia modes and an increased time step. As before, the phase speeds of the gravity-inertia modes are reduced everywhere in the stable region for $\alpha \geq 0.4$ (Figure 19).

Figures 20 and 21 illustrate the effect of reducing the mean geopotential while keeping α and β fixed at 0.35. As in the category 1 configuration, the intermediate instability area appears for small values of $\overline{\Phi}$. Here, the values of α and β needed to eliminate the undersired behavior is larger than the value α needed in the category 1 use. This is also in accordance with the results of Section II, for the requirement was $\alpha \geq 4/27$ for category 1 type use (Figure 1) while $\alpha = \beta \geq 1/4$ was needed for category 2 type use (Figure 7). Application of the generalized Okamura procedure

to both τ and $\tau-1$ fields thus appears to be an attractive choice, for strong, highly selective damping achieved while the time step may increased. Both uses of the semi-iterative method are testing using a free-surface barotropic model in the next section.

IV. Tests of the Semi-Iterative Method in a Free-Surface Barotropic Model

1. Experimental Design

The semi-iterative method was tested using a free-surface barotropic model. The finite difference equations are

$$\bar{u}_t^t - \overline{f\bar{v}^{xy} + g\bar{h}_x^y}^{xy} = -\overline{\bar{u}^{xy}\bar{u}_x^y - \bar{v}^{xy}\bar{u}_y^x}^{xy}, \tag{42}$$

$$\bar{v}_t^t + \overline{f\bar{u}^{xy} + g\bar{h}_y^x}^{xy} = -\overline{\bar{u}^{xy}\bar{v}_x^y - \bar{v}^{xy}\bar{v}_y^x}^{xy}, \tag{43}$$

$$\bar{h}_t^t + \overline{\bar{h}^{xy}\left[\bar{u}_x^y + \bar{v}_y^x\right]}^{xy} = -\overline{\bar{u}^{xy}\bar{h}_x^y - \bar{v}^{xy}\bar{h}_y^x}^{xy}, \tag{44}$$

where u and v are the horizontal wind components, h is the height, f is the coriolis parameter, and g is gravity. During the generalized Okamura iteration of the semi-iterative method, the right-hand side of (42)-(44) are set to zero. In two of the experiments, the Robert time filter was used. The time filter is of the form

$$\overline{S^n} = \gamma S^n + \frac{1-\gamma}{2}\left[S^{n+1} + \overline{S^{n-1}}\right], \tag{45}$$

where S is u, v, or h. The model was integrated on a 65x65 point Northern Hemisphere polar stereographic grid true at 60° north latitude. The grid interval was 381km.

A case was selected in which a closed cyclonic circulation developed over the western United States during a 5-day period. The initial time of the case was 1200 GMTt, 17 May, 1981. The initial analyses of u,v, and h were provided by the Hough global spectral analysis (Flattery, 1971). As a consequence, the initial mass and motion fields were related quasi-geostrophically and the initial divergence was nearly zero.

Initial imbalances between the mass and motion fields lead to generation of gravity-inertia wave noise. The various schemes were examined with respect to their comparative handling of both gravity-inertia wave noise and synoptic-scale meteorological scale motions.

Five 120 hour forecasts were made, differing only in the time integration method used. The five different time schemes were

Control: centered differences, Δt =10 min.

Comparison: centered differences, time filter with

$\gamma = 0.15, \Delta t$ = 8 min.

Experiment 1: Semi-Iterative Method, m=1, α =0.30, n=0, β=0, Δt=30 min.

Experiment 2: Semi-Iterative Method, m=1, α =0.30, n=0, β =0, time filter with γ =0.90, Δt=30 min.

Experiment 3: Semi-Iterative Method, m=n=1, $\alpha = \beta$= 0.45, Δt = 20 min.

2. Experimental Results

Consider first the graphs of RMS divergence and absolute vorticity shown in Figures 22 and 23. In the control run, the RMS divergence maintains a level of from 4×10^{-6} to 5×10^{-6} s^{-1} throughout the five days of the forecast. The use of the time filter with a strongly damping coefficient of 0.15 in the comparison run very effectively controls the gravity-inertia wave noise that was present in the control run. In Exp. 1, the RMS divergence decreases at first, then increases slowly. This is somewhat puzzeling, since the analysis of Section III indicated no damping for this choice. As will be seen shortly, the five day forecast maps produced by Exp. 1 were extremely noisy in appearance, much more so than in the control run. For this reason, the forecast was rerun using the time filter with a coefficient of 0.9. This forecast is designated

Exp. 2. Note that this did not necessitate a reduction of the 30 min. time step of Exp. 1. It did, however, control the noise. In Exp. 3, the noise was controlled slightly better than even in the comparison run. The RMS absolute vorticity decreased in Exps. 2 and 3 and the comparison run more than in either the control run or Exp. 1, although the amount was small. The increased reduction of RMS absolute vorticity was to be expected in the comparison run and Exp. 2 due to use of the time filter, which is not a very selective noise damper. It was not expected in Exp. 3.

The forecast 500mb height maps are shown in Figures (24)-(29) (for a portion of the grid). Here, we note a noisy map from the control run (figure 24) and an extremely noisy map from Exp. 1 (Figure 26). The noise is completely eliminated by use of the time filter in Exp. 2 (Figure 27). The maps from the comparison run and Exp. 3 are also noisefree. The central depth of the closed circulation is lowest in Exp. 2 and highest in Exp. 1. It is disappointing to note that the low is not as deep in Exp. 3 (Figure 28) as in the control run or even the comparison run (Figure 25). The maps of wind speed and absolute vorticity (not shown) confirm a slight but consistent loss of amplitude in the five day forecast of the synoptic-scale features in Exp. 3. This is both puzzeling and disturbing, for it seems to disagree with the analysis in Section III. The maximum allowable time step, however, was determined experimentally to agree quite well with the indications in Section III in all five forecasts.

3. Assessment of the Experimental Results

Use of the semi-iterative method can provide either an increased time step with no damping or a smaller increase time step with strong

damping. The computer time (CPU) required for each 120 hour forecast was:

Control Run	96 sec.
Comparison Run	121 sec.
Experiment 1	65 sec.
Experiment 2	65 sec.
Experiment 3	99 sec.

Thus, the Semi-Iterative Method proves to be quite efficient. The saving of computer time would be even greater in a complex baroclinic model, for the physics would only have to be computed one-half (Exp. 3) or one-third (Exps. 1 and 2) as often as normally. The damping of the Semi-Iterative Method is also substantial, whether provided by the time filter, as in Exp. 2, or by the choice of parameters, as in Exp. 3. In this sense, the Semi-Iterative Method indeed proves to be an efficient and effective noise control device, as suggested in Section II.

Several notes of caution must, in fairness, be added to this assessment. First, the damping in Exp. 3 does not seem to be as selective as was hoped at the outset and indicated by the linear analysis, for there was a disturbing amount of damping of the synoptic-scale meteorological motions. Furthermore, although use of the time filter in Exp. 2 did control the extreme amount of noise noted in Exp. 1, it must be remembered that this is only a barotropic model. The noise apparently present in Exp. 1 could therefore be easily controlled by the time filter. It is possible that application of this form of the Semi-Iterative Method to a baroclinic model would result in internal gravity-inertia wave noise that could not be so easily controlled with the time filter. One more factor must also be pointed out. The Semi-Iterative Method requires an extra set

of fields. This would increase the storage requirements of a model unless some appropriate reading in and writing out of fields was used.

V. Concluding Remarks

The generalized Okamura procedures is a potent damping device. This paper described a methodd of incorporating this device into centered time differences. The result is an increased time step and strong damping.

One drawback lies in increased storage requirements, although creative programming might at least alleviate this. A more serious problem lies in the selectivity of the damping. The results of Experiments 1, 2, and 3 suggest to me that the source of the problem might lie in an imprecise identification of the terms driving the gravity-inertia wave motions to which the generalized Okamura technique is applied. If future research could eliminate this drawback, the Semi-Iterative Method would become a very attractive candidate for numerical weather prediction models.

REFERENCES

Flattery, T., 1971: Spectral models for global analysis and forecasting. Proc. Sixth AWS Technical Exchange Conference, U.S. Naval Academy, Annapolis, MD., 21-24 September 1970. Air Weather Service Tech Re. 242, 42-54.

Grant, W.F.K., 1974: On initialization of primative equation models, M.S. Thesis, Mass. Institute of Technology, 67pp.

Kurihara, Y., 1965: On the use of implicit and iterative methods for the time integration of the wave equation, Mon. Wea Rev., 93, 33-46.

_____, and G. J. Tripoli, 1976: An iterative time intergration scheme designed to preserve a low-frequency wave, Mon. Wea. Rev., 104, 761-764.

Matsuno, 1966: Numerical integrations of the primitive equations by a simulated backward difference method, J. Meteor. Soc Japan, 44, 76-84.

Nitta, T., 1969: Initialization and analysis for the primative equation model. Proc. Int. WMO/IUGG Symp Numerical Weather Prediction, Tokyo, Meteor. Soc. Japan, pp. VI-11 to VI-20.

Robert, A., 1966: The integration of a low order spectral form of the primitive meteorological equations, J. Meteor. Soc. Japan, 44, No. 5.

K+E 10 X 10 TO ½ INCH 46 1320
7 X 10 INCHES MADE IN U.S.A.
KEUFFEL & ESSER CO.

Figure 1

α_+ and α_- for OR applied to ϕ^τ

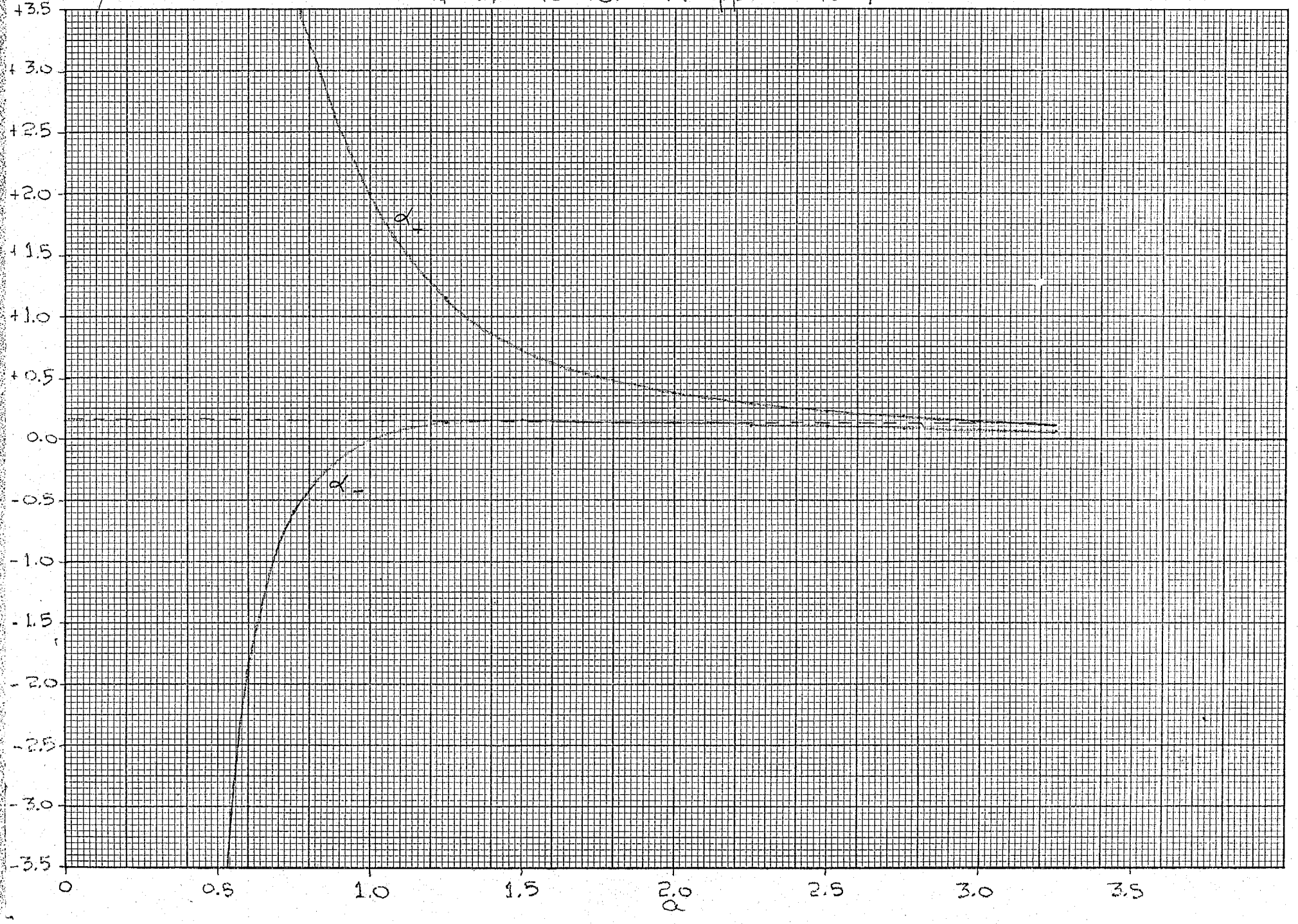

K+E 10 X 10 TO ½ INCH 46 1320
7 X 10 INCHES MADE IN U.S.A.
KEUFFEL & ESSER CO.

Figure 2. Amplitude of physical and computational Modes; OR applied to ϕ^{μ} (For $\alpha = 4/27$)

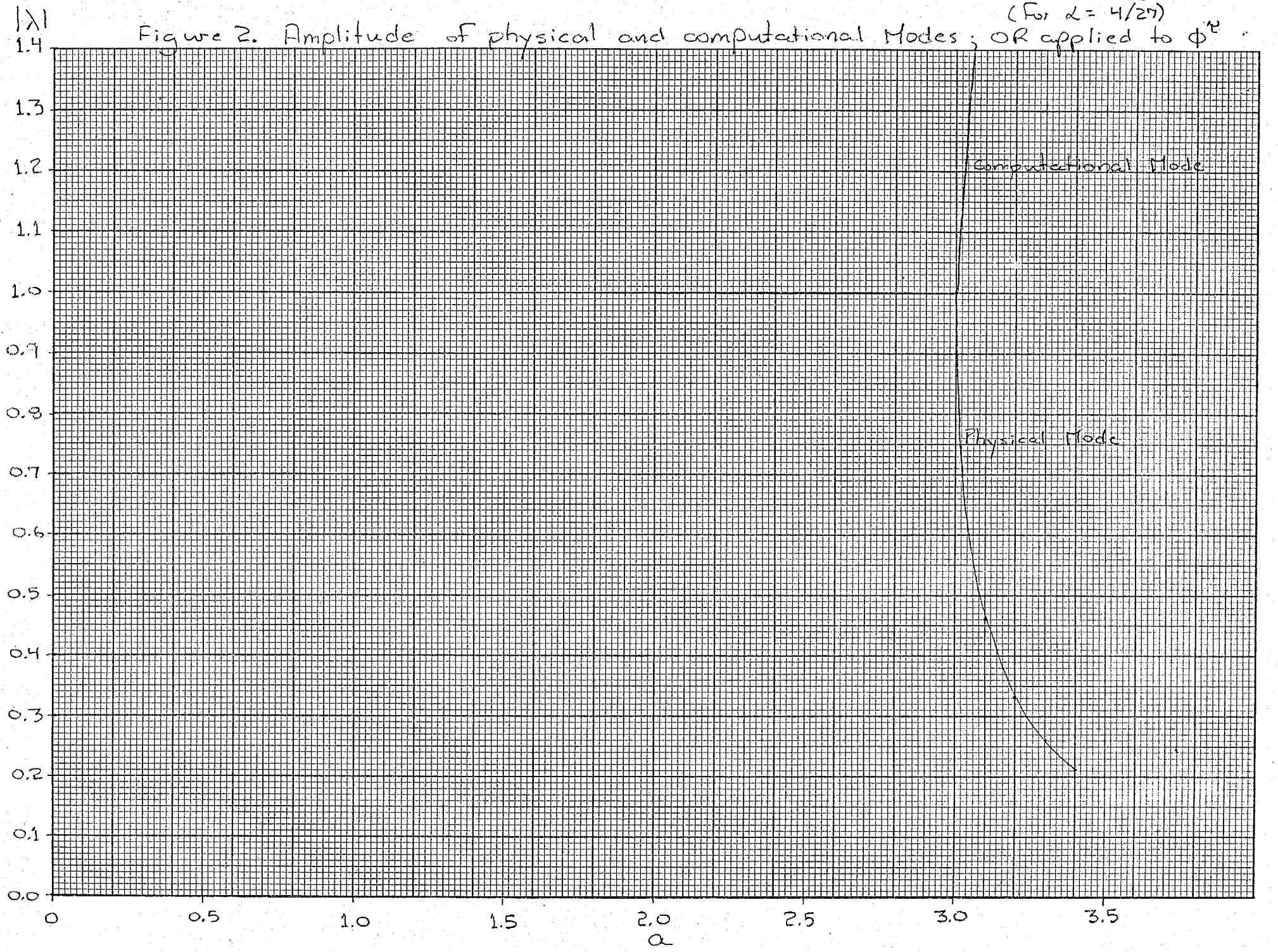

K+E 10 X 10 TO ½ INCH 46 1320
7 X 10 INCHES MADE IN U.S.A.
KEUFFEL & ESSER CO.

(For $\alpha = 4/27$)

Figure 3. Ratio of Numerical to Analytic Phase Speeds for Physical and Computational Modes; OR applied to

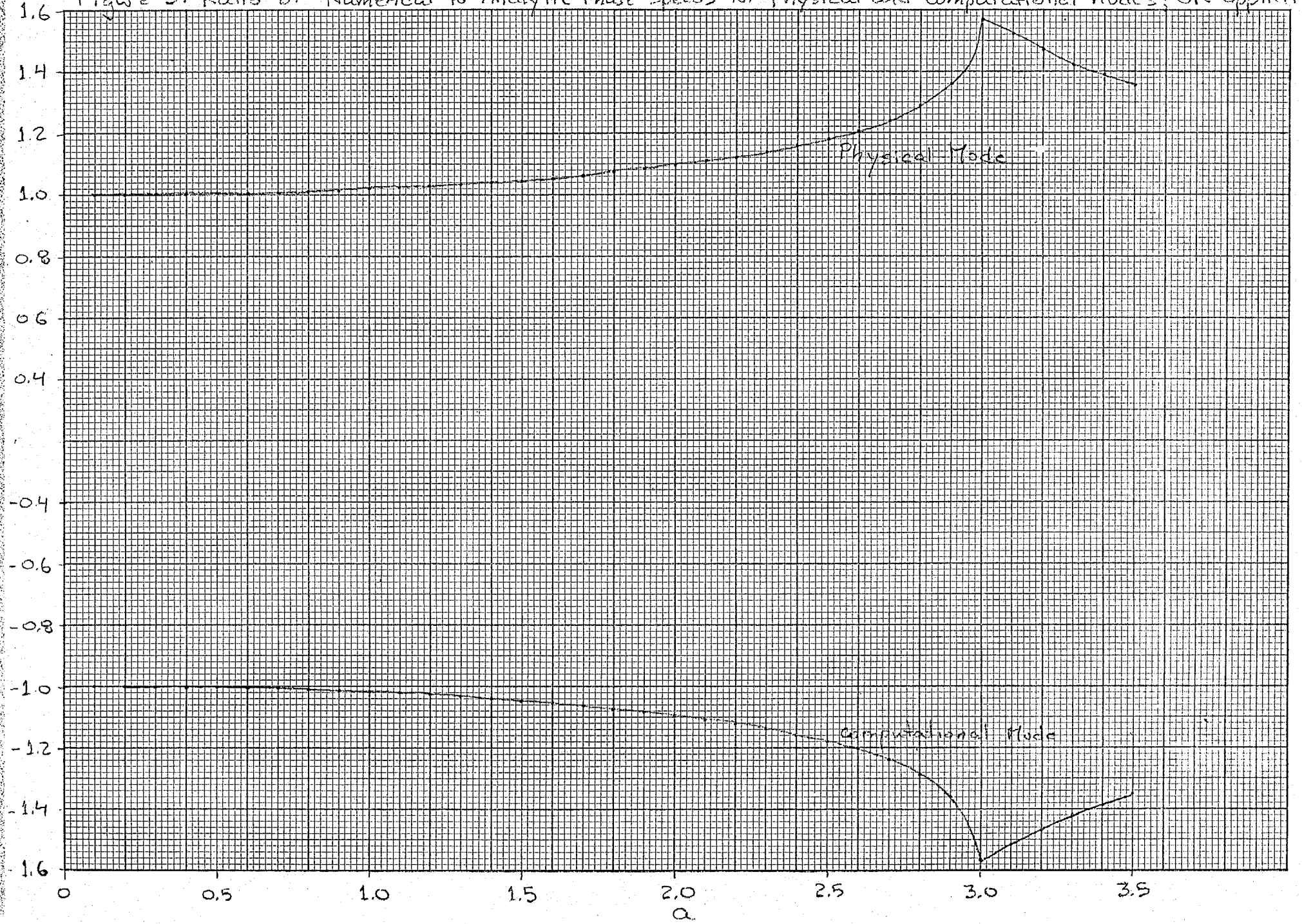

K+E 10 X 10 TO ½ INCH 46 1320
7 X 10 INCHES MADE IN U.S.A.
KEUFFEL & ESSER CO.

Figure 4. α_{max} for OR applied to $\phi^{\tau-1}$

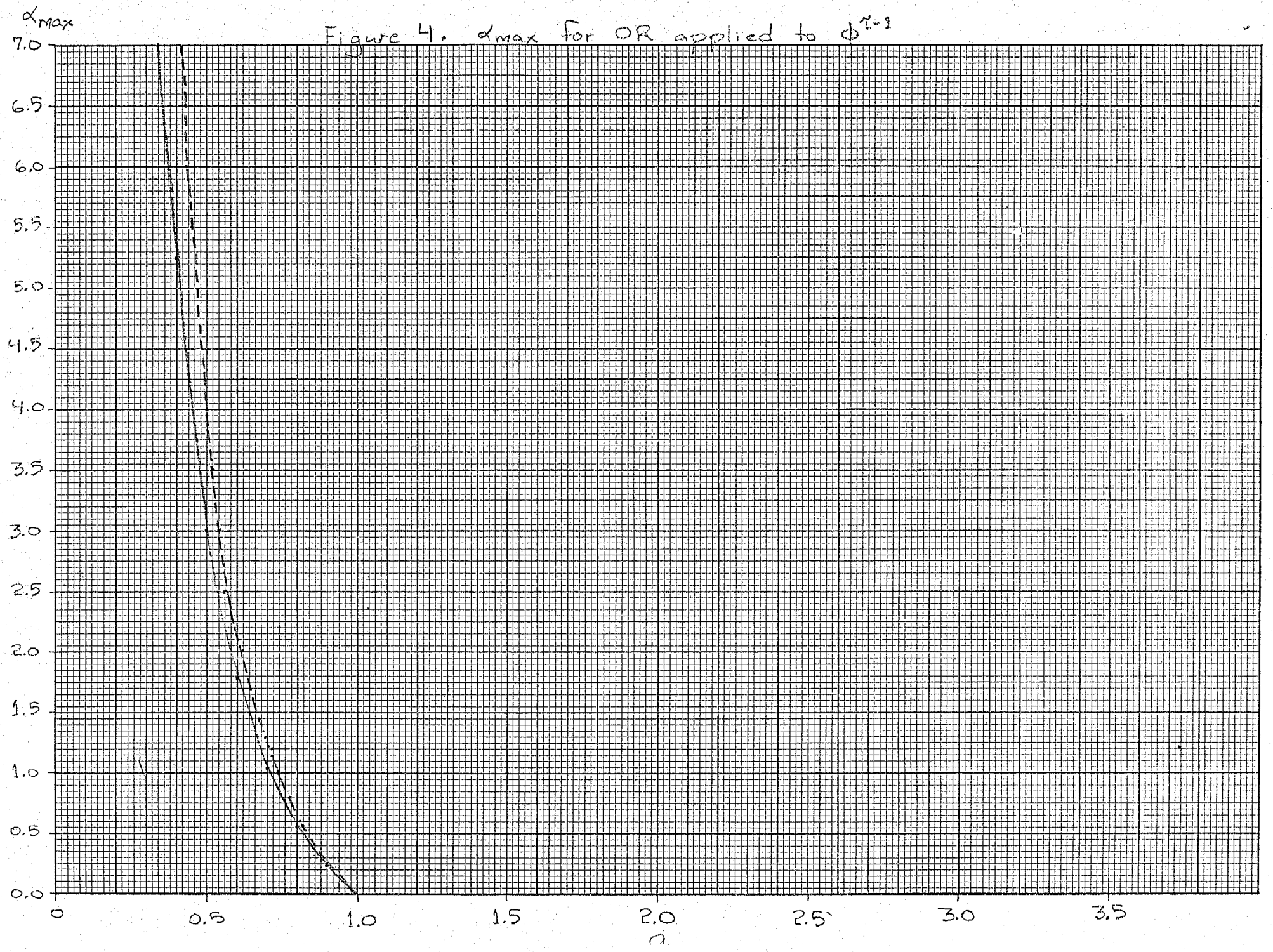

K+E 10 X 10 TO ½ INCH 46 1320
7 X 10 INCHES MADE IN U.S.A.
KEUFFEL & ESSER CO.

Figure 5. Amplitude of physical and computational modes for $\alpha = 1.0$; OR applied to ϕ^{n-1}.

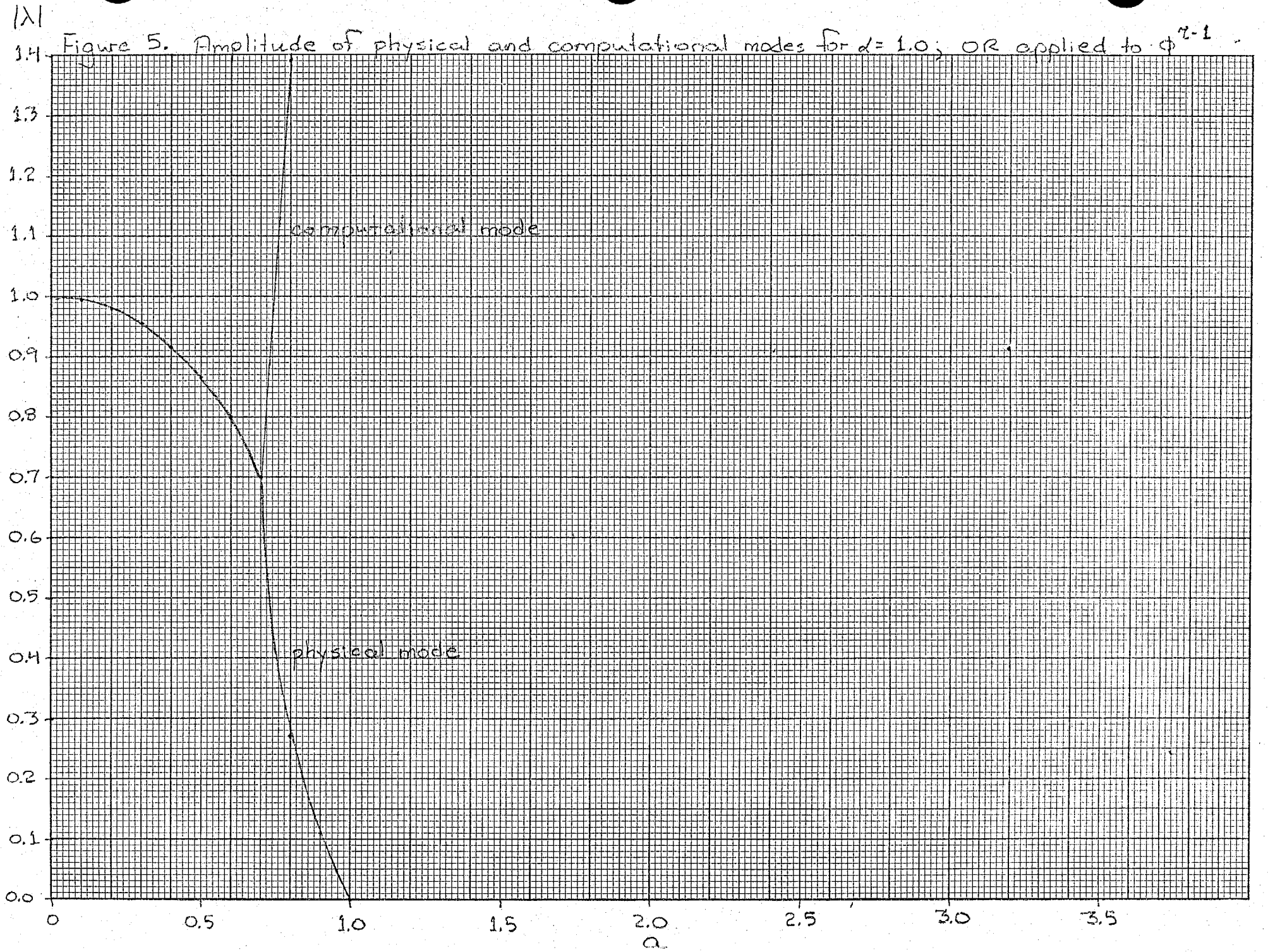

K+E 10 X 10 TO ½ INCH 46 1320
7 X 10 INCHES MADE IN U.S.A.
KEUFFEL & ESSER CO.

Figure 6. Ratio of Numerical to Analytic Phase Speeds for physical and computational modes for $\alpha = 1.0$; to ϕ

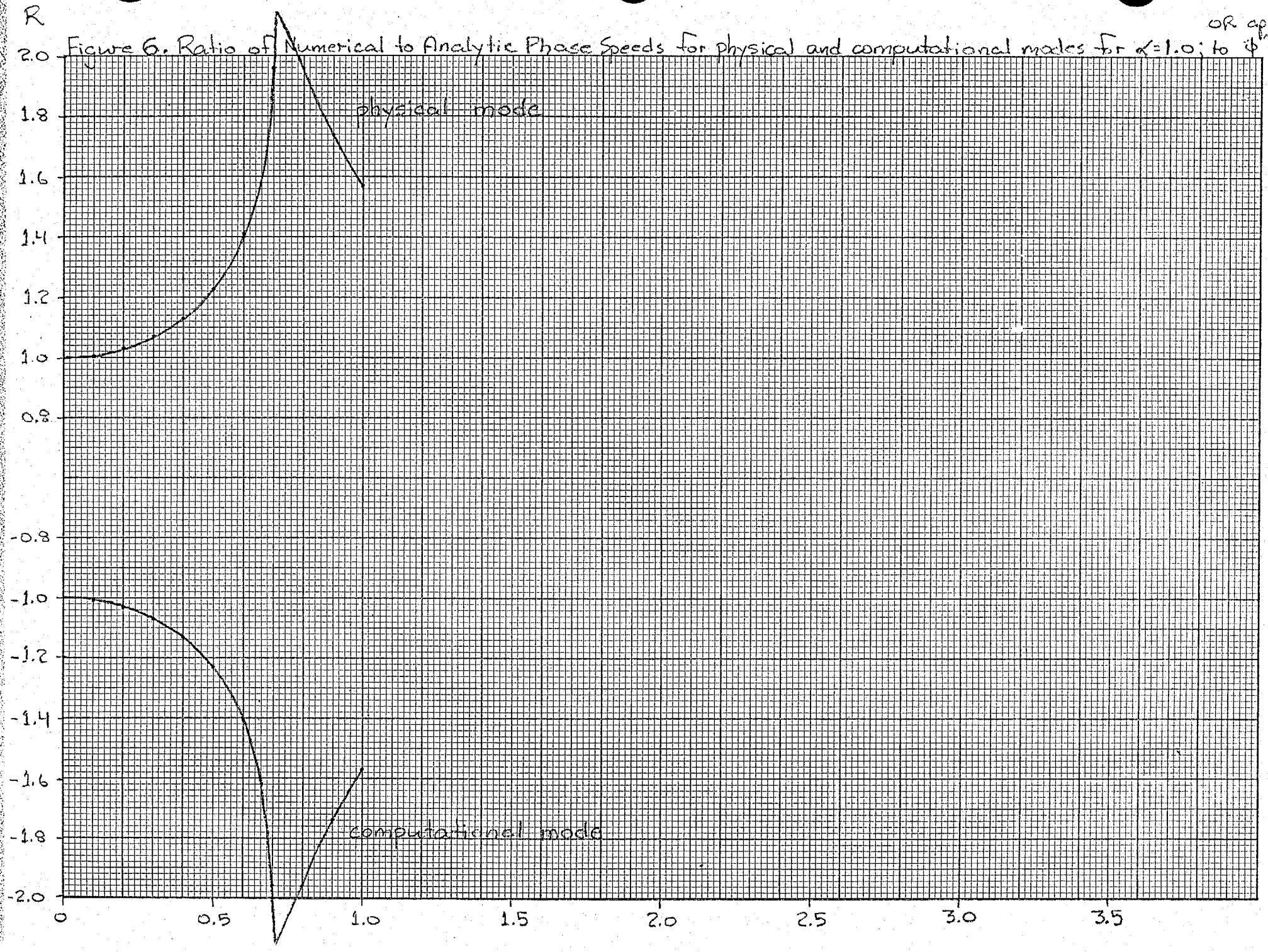

K+E 10 X 10 TO ½ INCH 46 1320
7 X 10 INCHES MADE IN U.S.A.
KEUFFEL & ESSER CO.

Figure 7. α_+ and α_- for OR applied to ϕ^{τ} and $\phi^{\tau-1}$

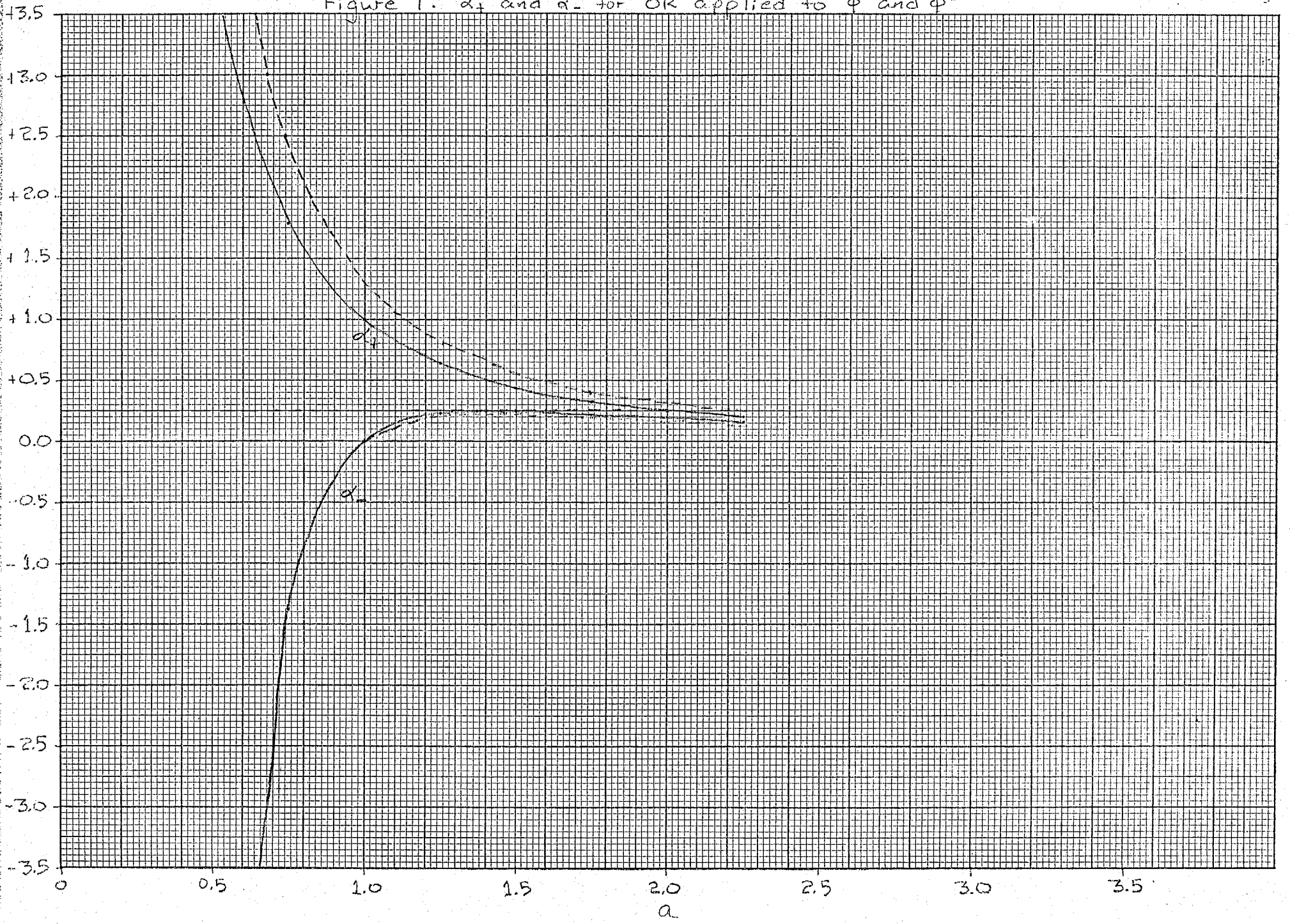

K+E 10 X 10 TO ½ INCH 46 1320
7 X 10 INCHES MADE IN U.S.A.
KEUFFEL & ESSER CO.

Figure 8. Amplitude of physical and computational modes for $\alpha = 0.25$; OR applied to ϕ^{ξ} and

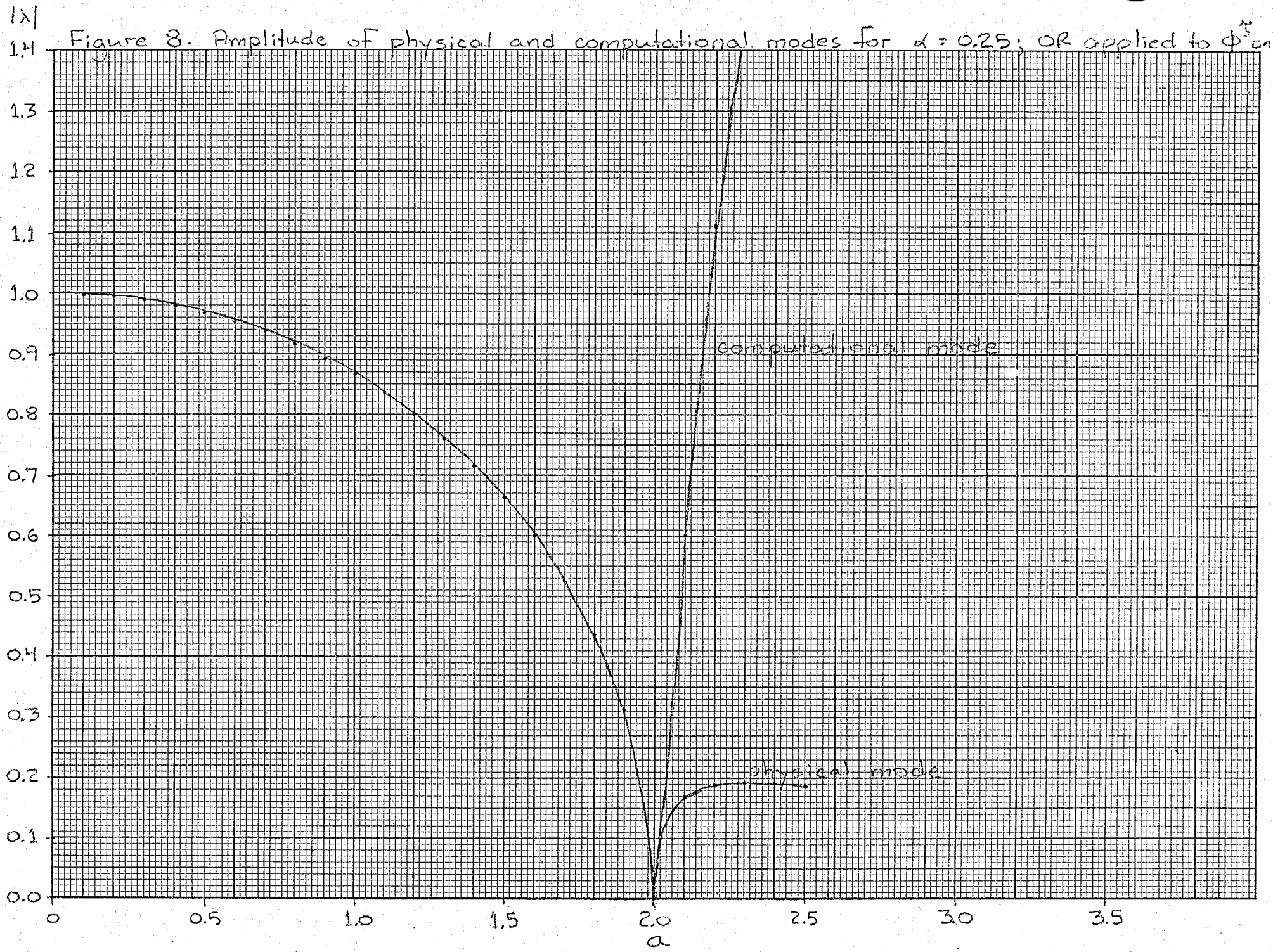

K+E 10 X 10 TO ½ INCH 46 1320
7 X 10 INCHES MADE IN U.S.A.
KEUFFEL & ESSER CO.

Figure 9. Ratio of numerical to analytic phase speed for physical and computational modes for $\alpha = 0.25$; ϕ^c and ϕ^{c*} OR applied to

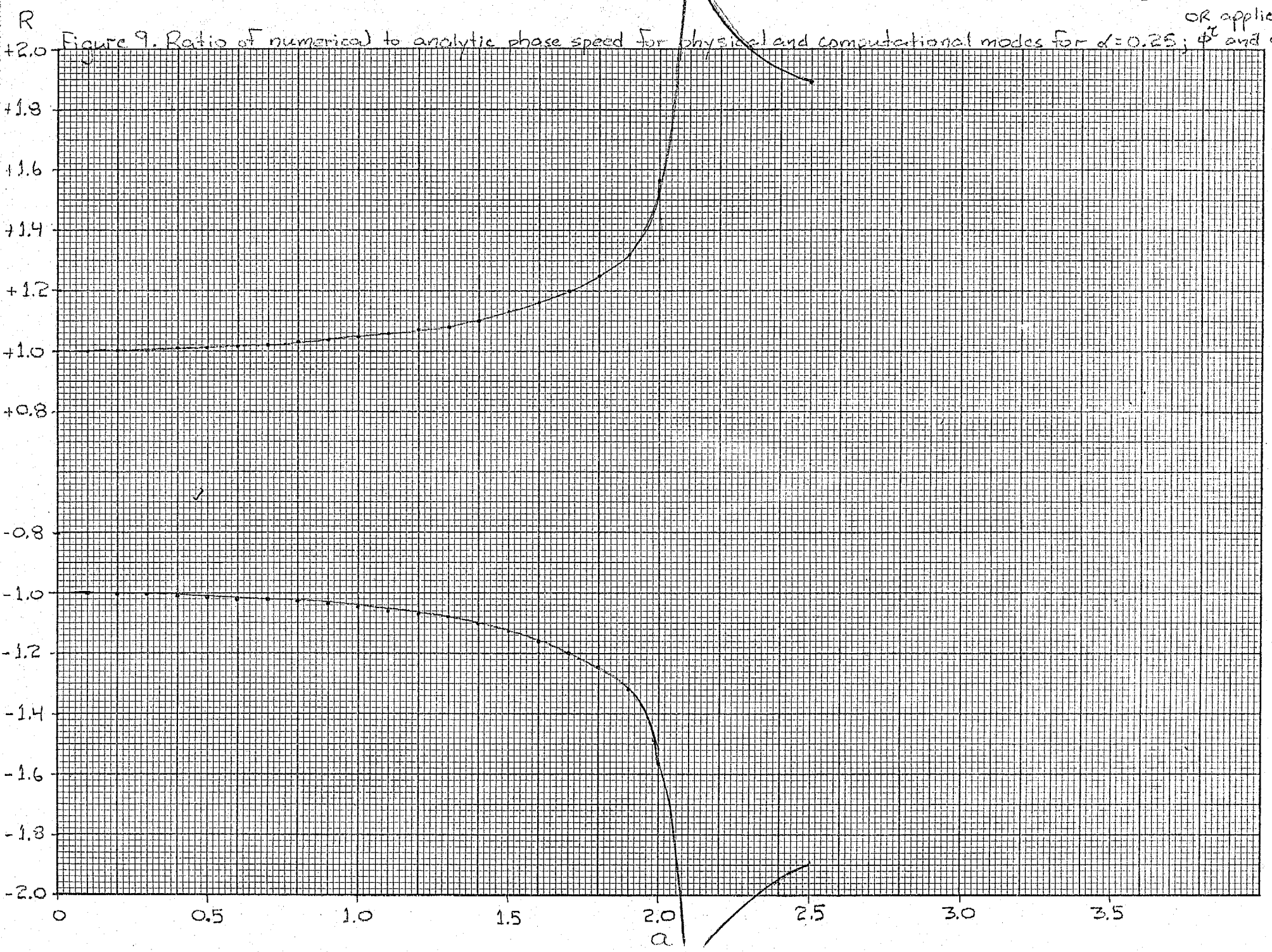

K+E 10 X 10 TO ½ INCH 46 1320
7 X 10 INCHES MADE IN U.S.A.
KEUFFEL & ESSER CO.

Figure 10: Amplitude of physical and computational meteorological modes: OR on ϕ^{τ} only

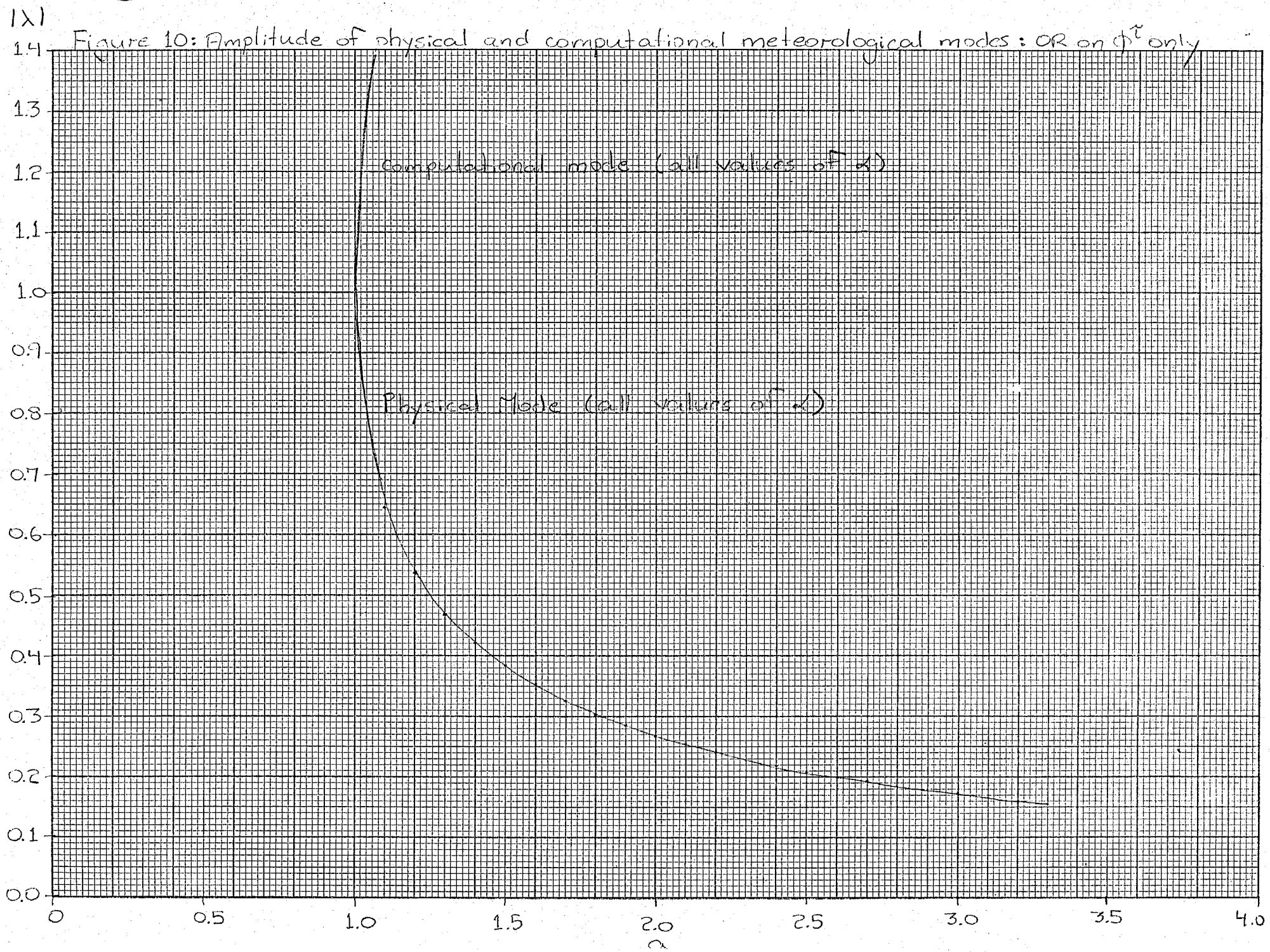

K+E 10 X 10 TO ½ INCH 46 1320
7 X 10 INCHES MADE IN U.S.A.
KEUFFEL & ESSER CO.

(OK on ϕ^t only)

Figure 11: Ratio of Numerical to Analytic Phase Speeds for Physical and Computational Meteorological Mo

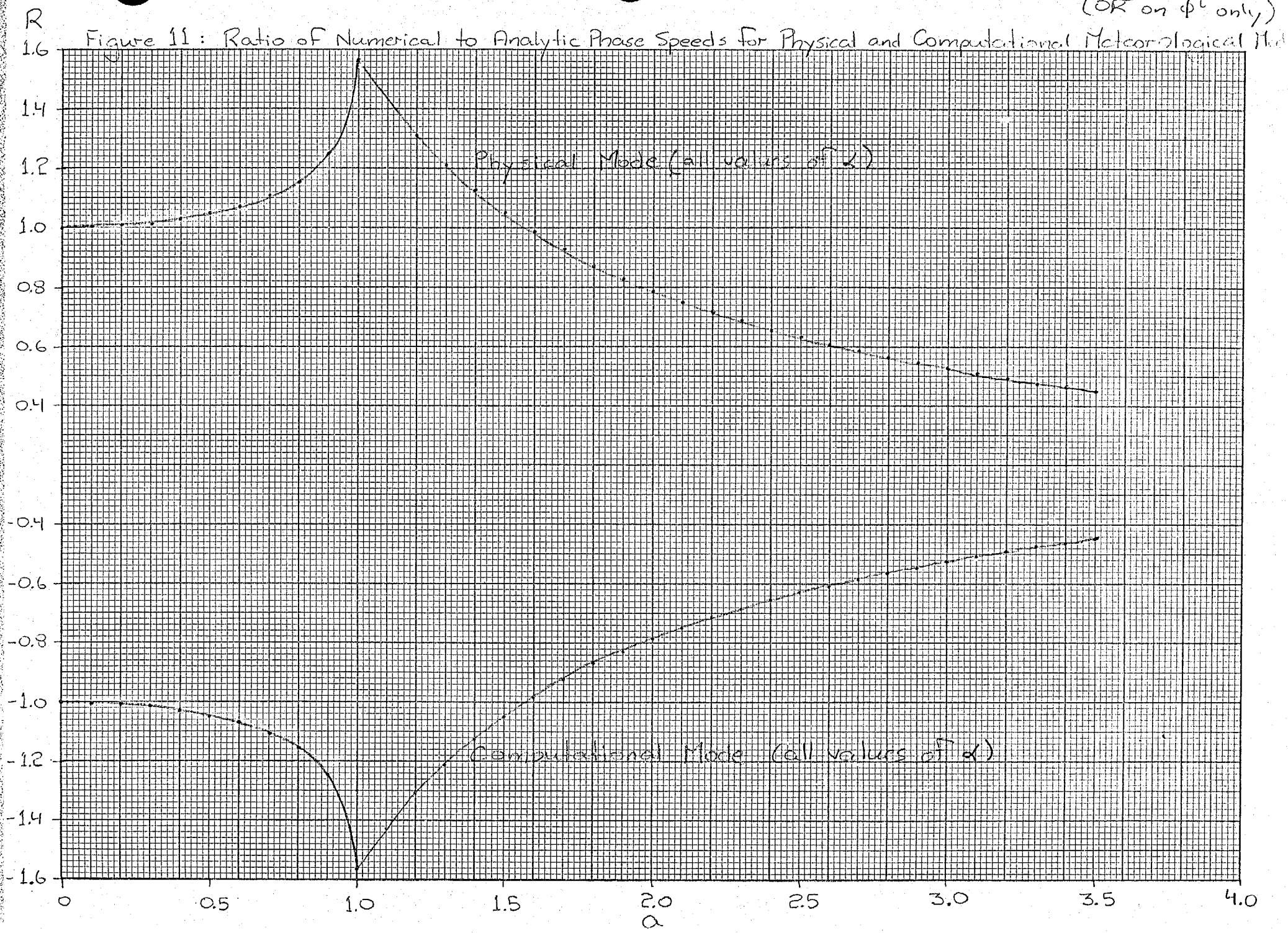

K+E 10 X 10 TO ½ INCH 46 1320
7 X 10 INCHES MADE IN U.S.A.
KEUFFEL & ESSER CO.

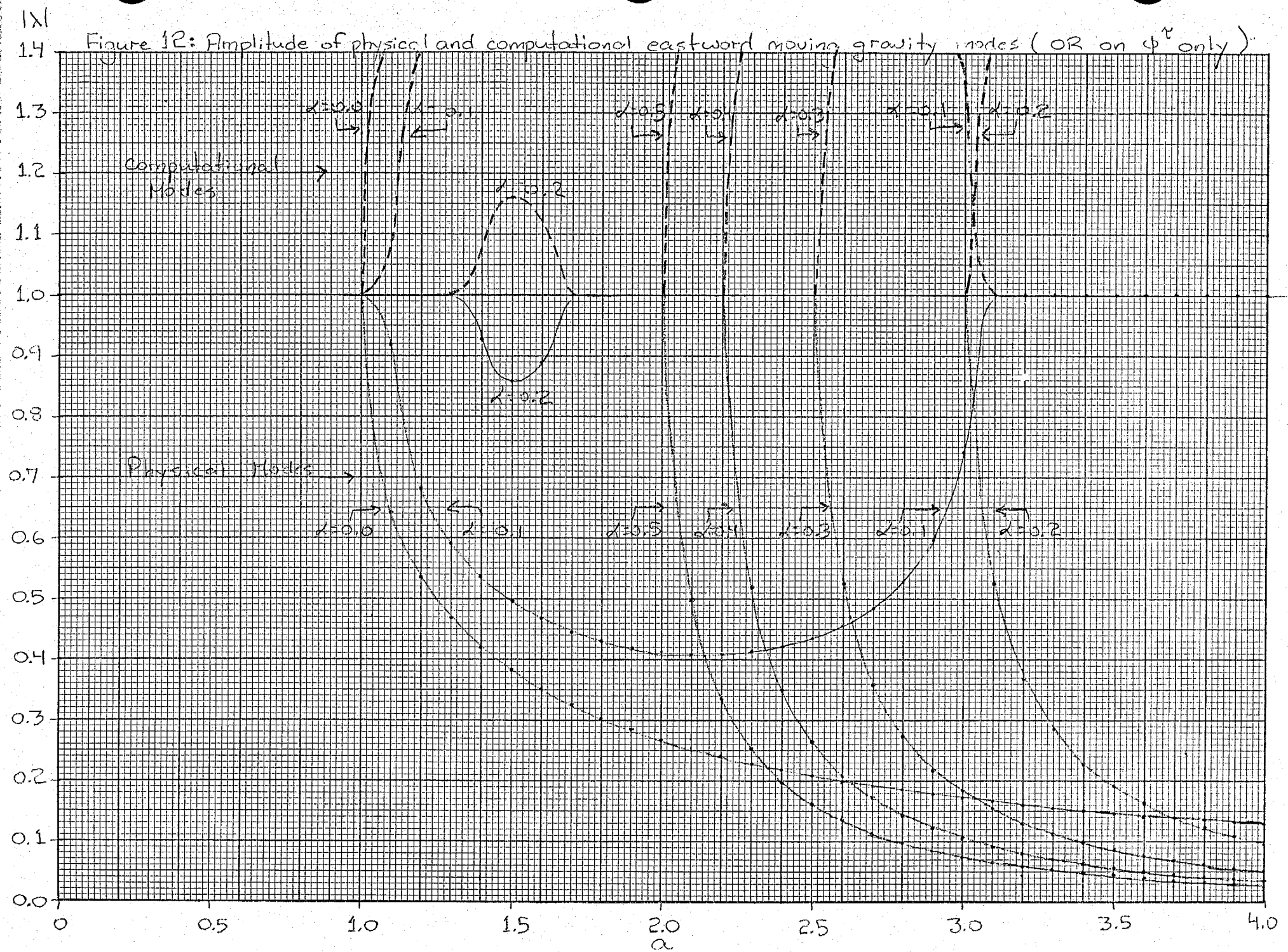

Figure 12: Amplitude of physical and computational eastward moving gravity modes (OR on ϕ^{τ} only)

K+E 10 X 10 TO ½ INCH 46 1320
7 X 10 INCHES MADE IN U.S.A.
KEUFFEL & ESSER CO.

Figure 13: Ratio of Numerical to Analytic Phase Speeds for Physical and Computational Eastward Moving Gravity Modes (OR on ϕ^{τ} only)

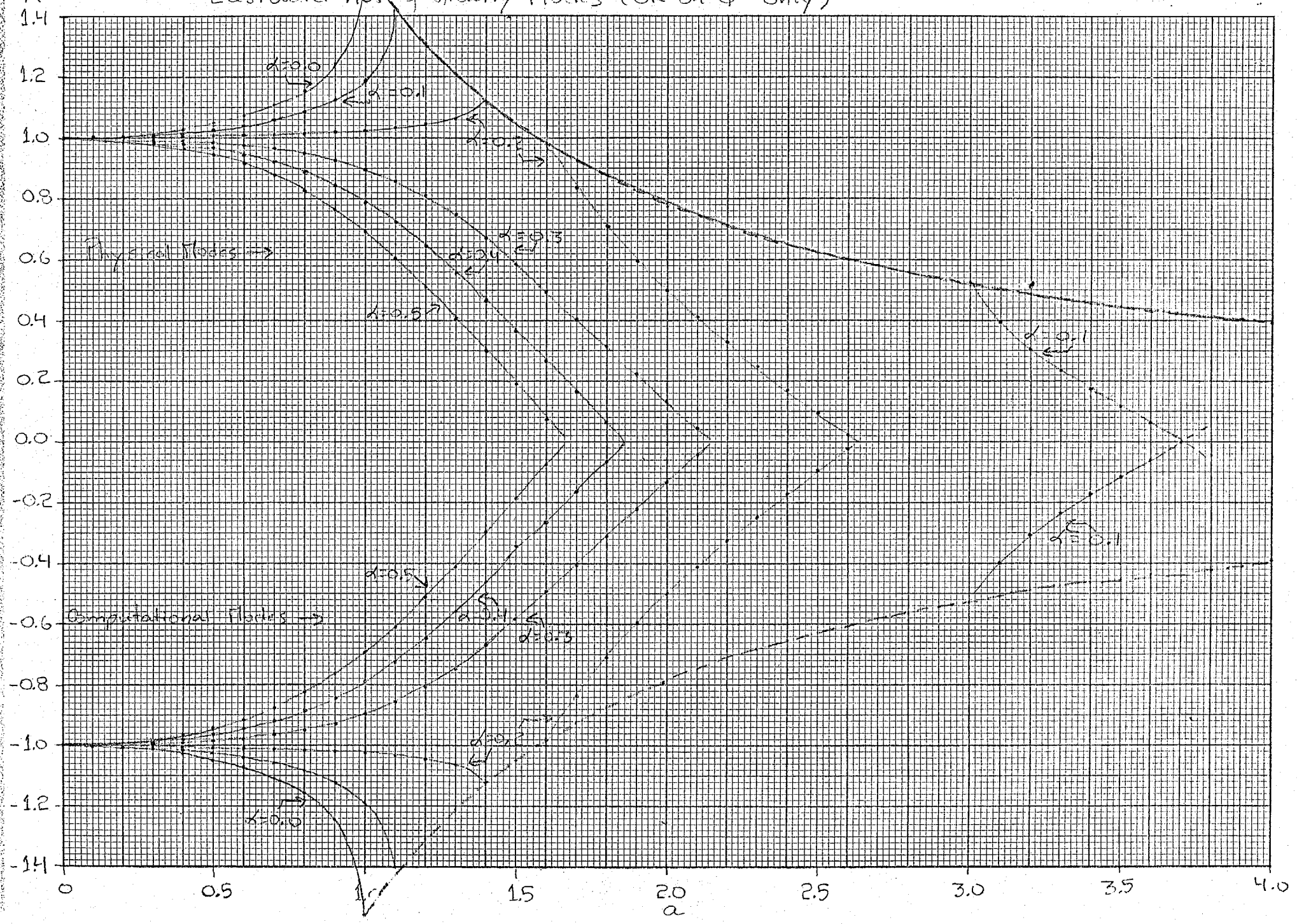

K+E 10 X 10 TO ½ INCH 46 1320
7 X 10 INCHES MADE IN U.S.A.
KEUFFEL & ESSER CO.

Figure 14: Amplitude of physical and computational eastward moving gravity modes (OR on ϕ^{τ} only, $\alpha = .25$

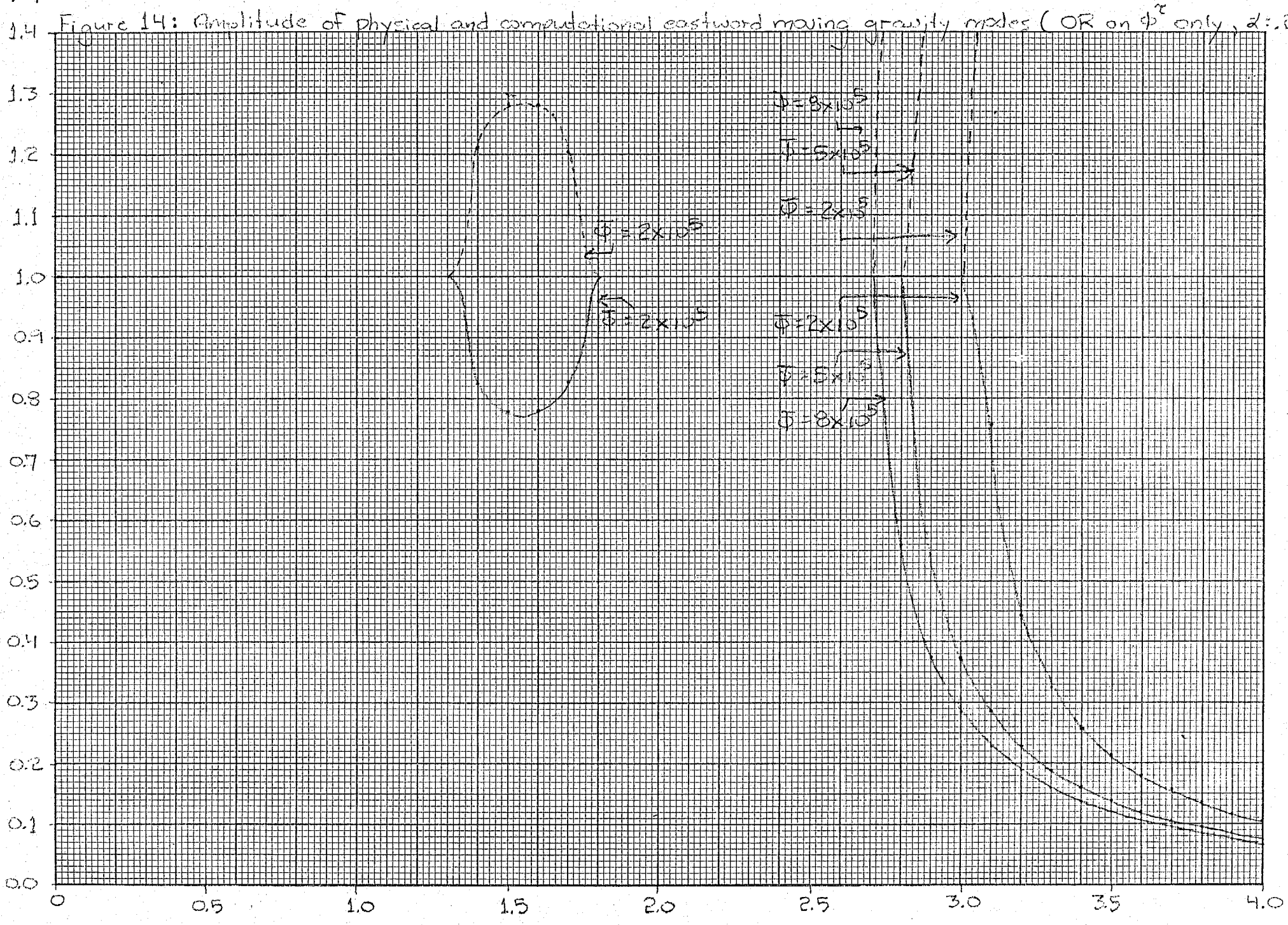

K+E 10 X 10 TO ½ INCH 46 1320
7 X 10 INCHES MADE IN U.S.A.
KEUFFEL & ESSER CO.

Figure 15: Ratio of Numerical to Analytic Phase Speed for Physical and Computational Eastward Moving Gravity Modes (OR on ϕ^{τ} only, $\alpha = 0.25$)

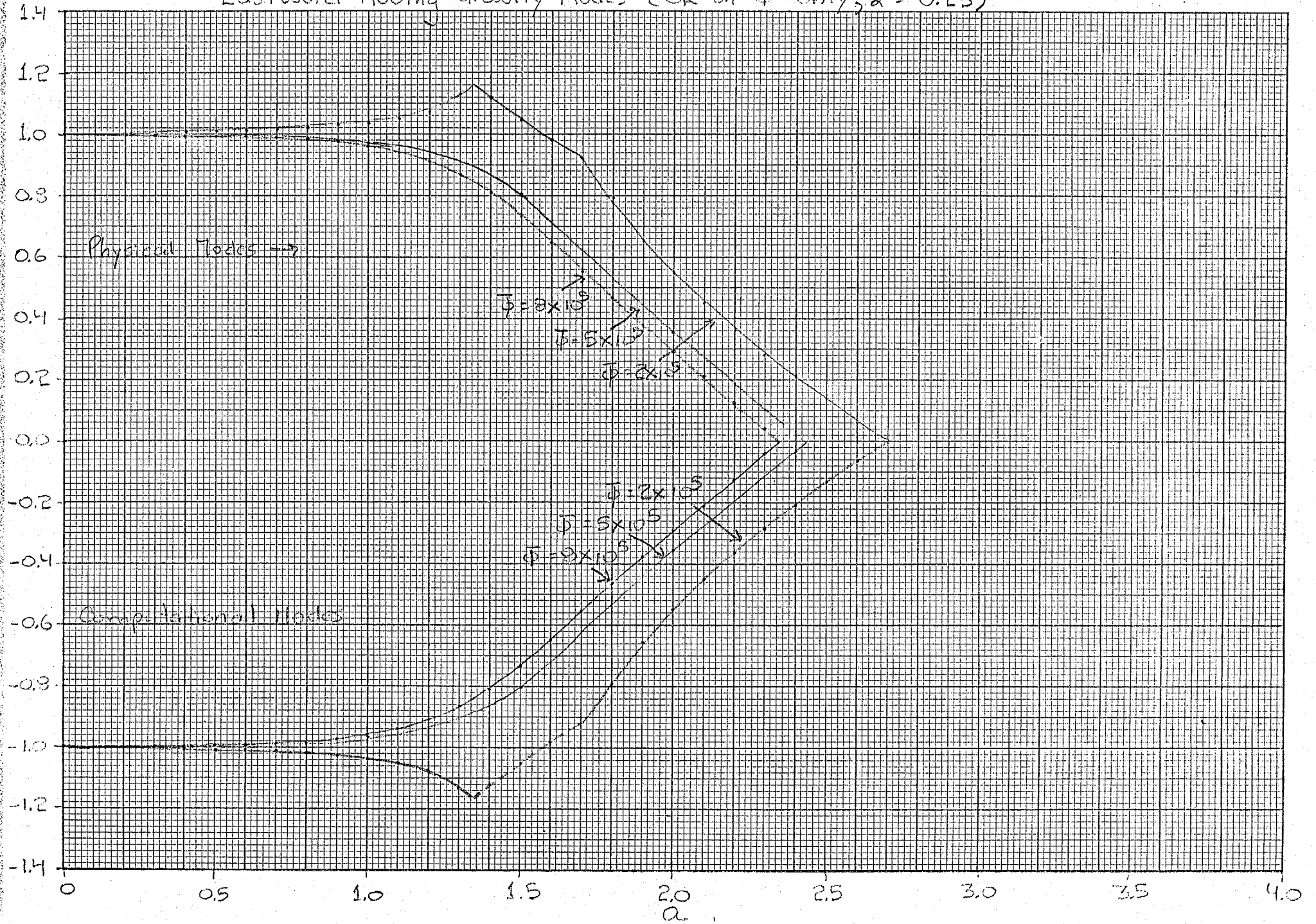

K+E 10 X 10 TO ½ INCH 46 1320
7 X 10 INCHES MADE IN U.S.A.
KEUFFEL & ESSER CO.

Figure 16: Amplitude of physical and computational meteorological modes (OR on ϕ^{τ} and $\phi^{\tau-1}$)

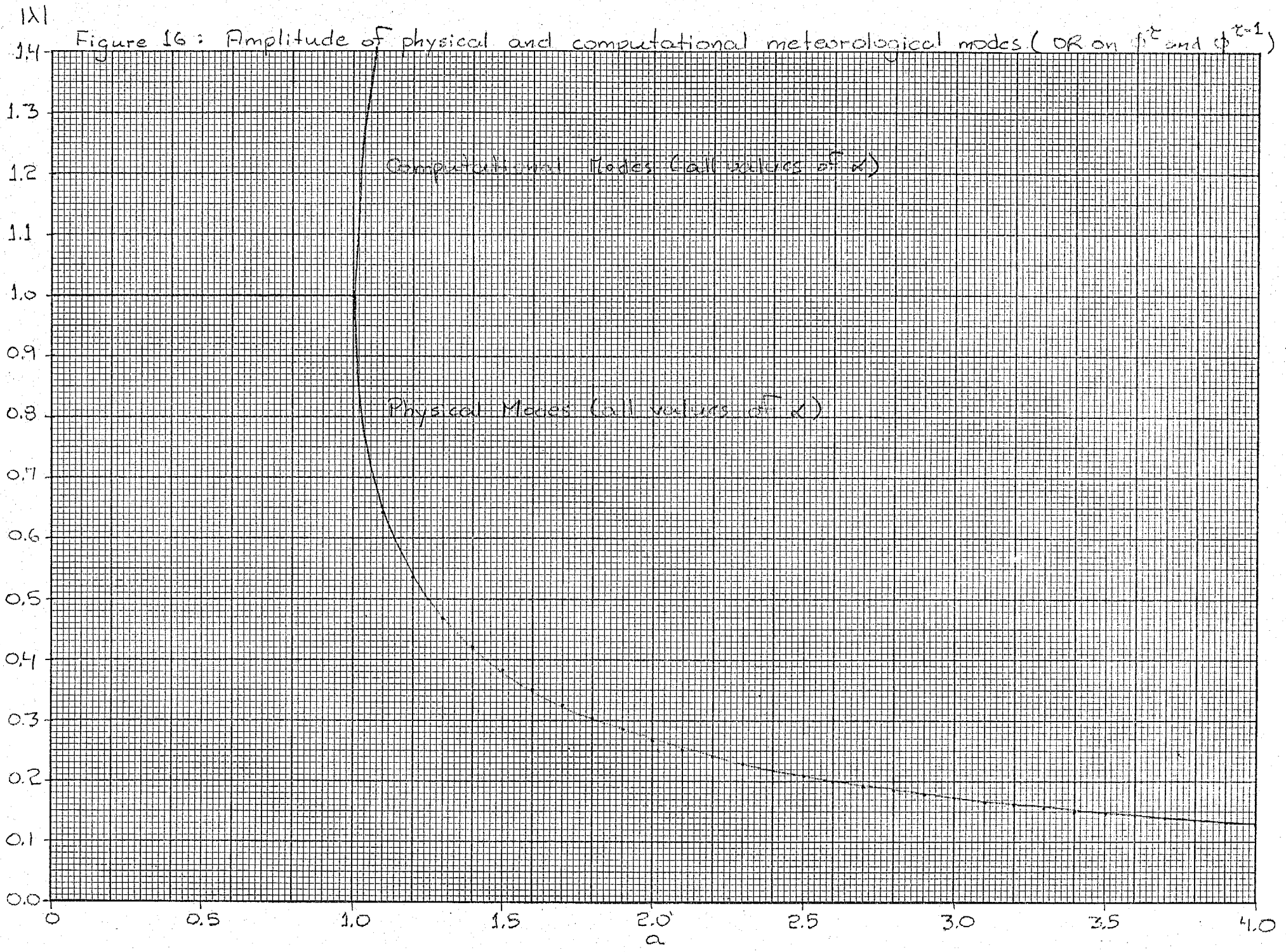

K+E 10 X 10 TO ½ INCH 7 X 10 INCHES. 4G 1320 MADE IN U.S.A. KEUFFEL & ESSER CO.

R Figure 17: Ratio of Numerical to Analytic Phase Speed for Physical and Computational Meteorological Modes (OR on ϕ^{τ} and $\phi^{\tau-1}$).

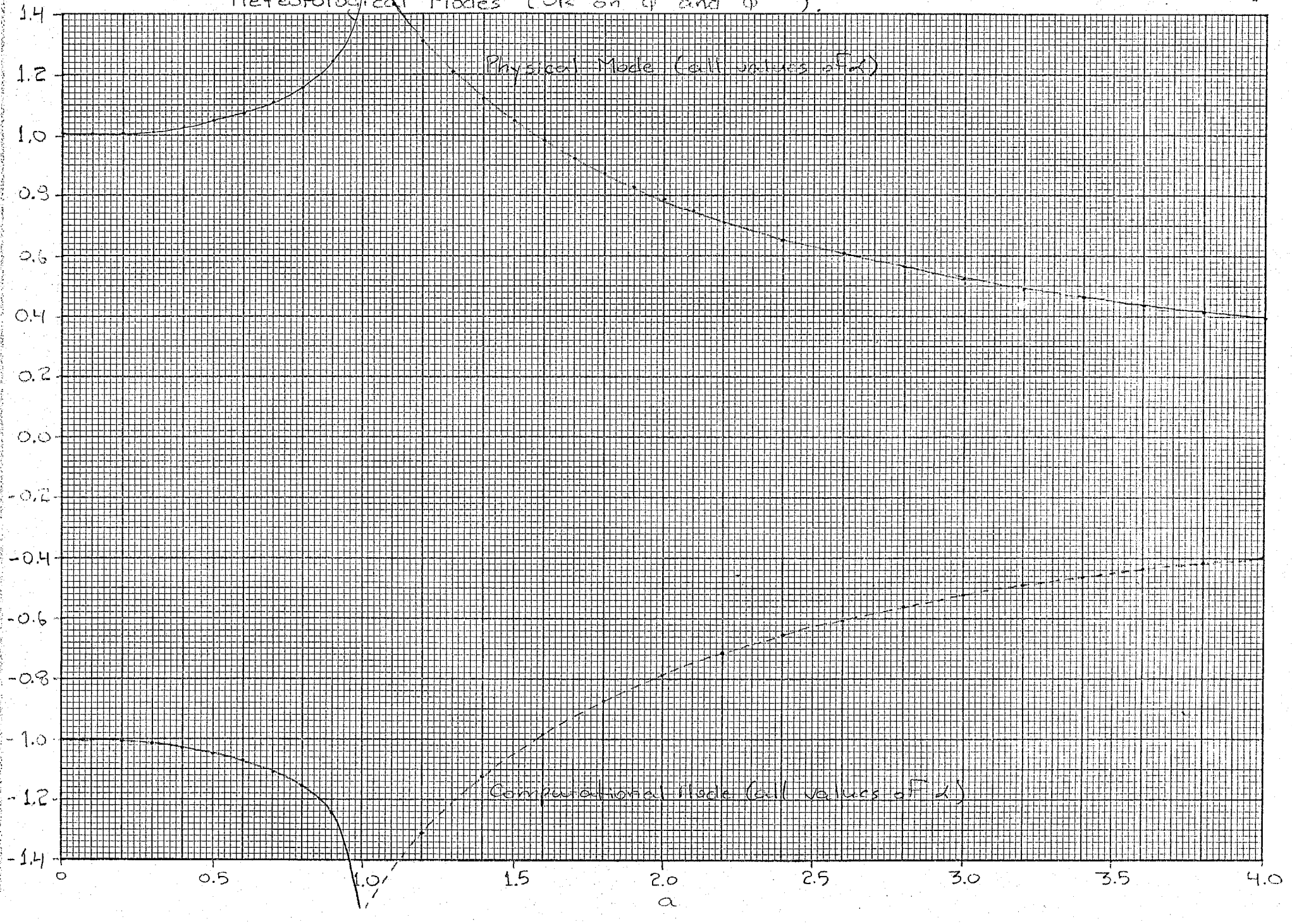

K+E 10 X 10 TO ½ INCH 46 1320
7 X 10 INCHES MADE IN U.S.A.
KEUFFEL & ESSER CO.

Figure 18: Amplitude of physical and computational eastward moving gravity modes (OR on ϕ^{γ} and $\phi^{\gamma-1}$)

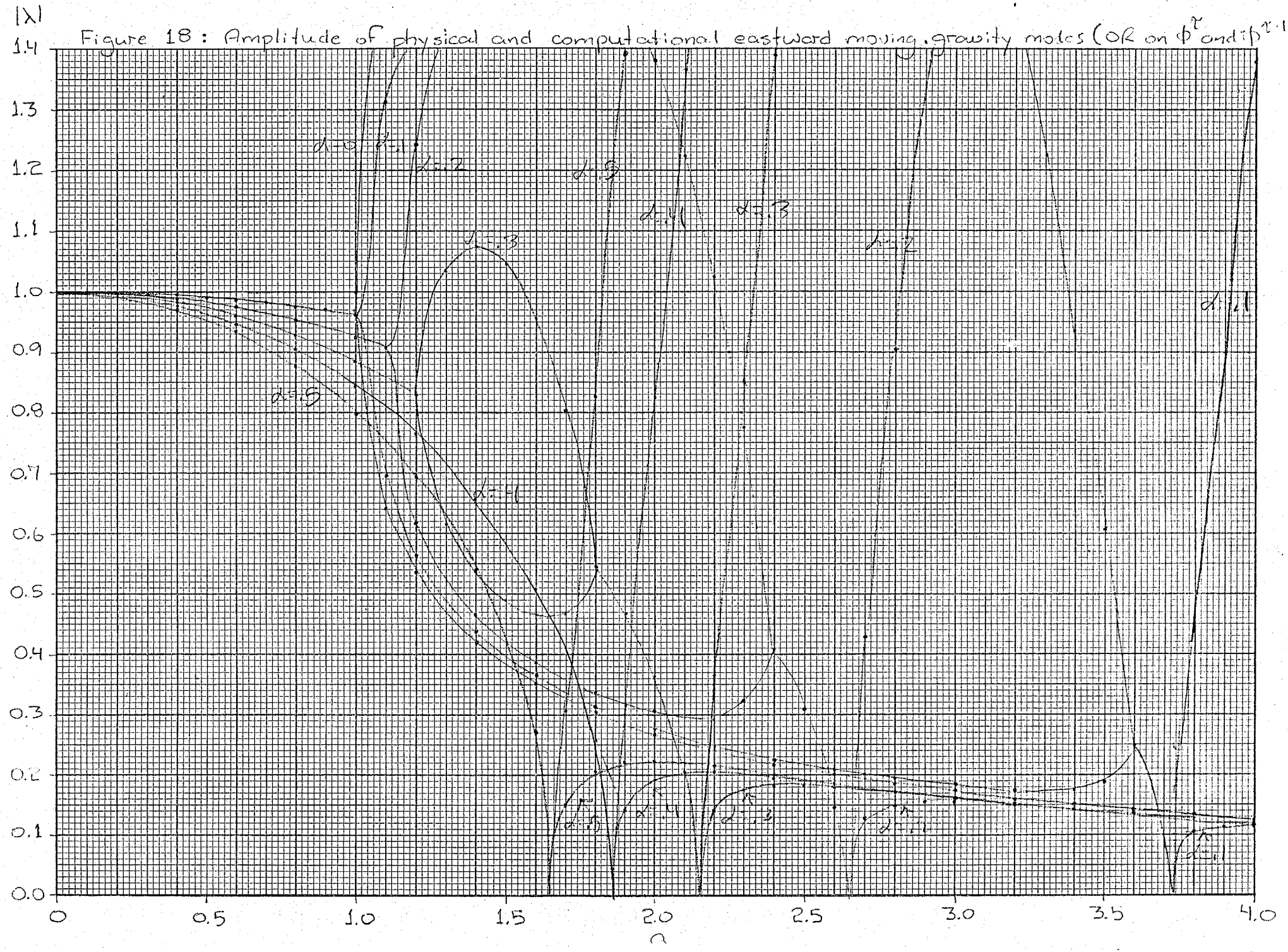

K+E 10 X 10 TO ½ INCH 46 1320
7 X 10 INCHES MADE IN U.S.A.
KEUFFEL & ESSER CO.

Figure 19: Ratio of Numerical to Analytic Phase Speeds for Physical and Computational Eastward Moving Gravity Modes (OR on ϕ^{τ} and $\phi^{\tau-1}$)

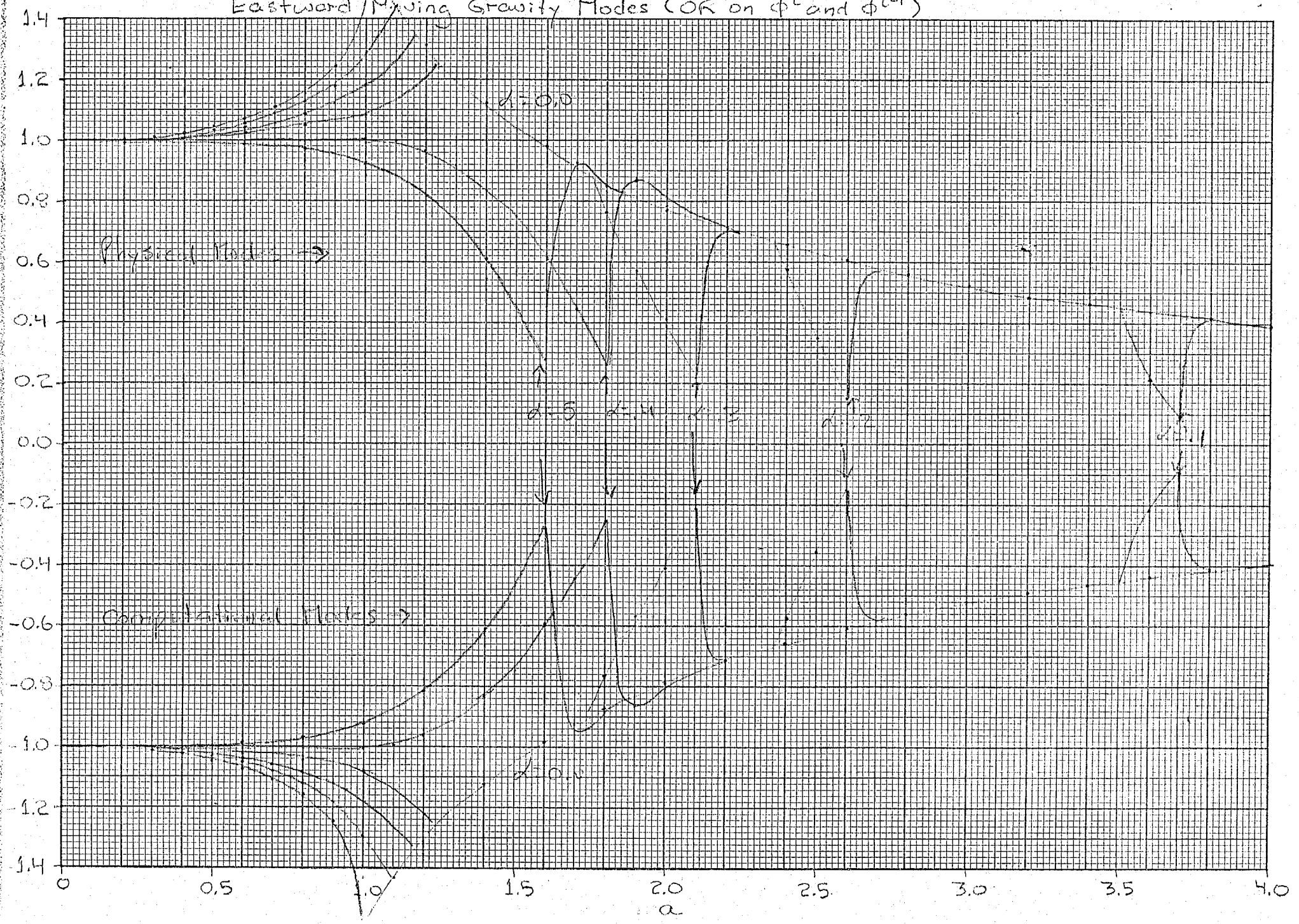

K+E 10 X 10 TO ½ INCH 46 1320
7 X 10 INCHES MADE IN U.S.A.
KEUFFEL & ESSER CO.

Figure 20: Amplitude of Physical and computational eastward moving gravity modes (OR on ϕ^{τ} + ϕ^{τ_1}), $\alpha = .3$

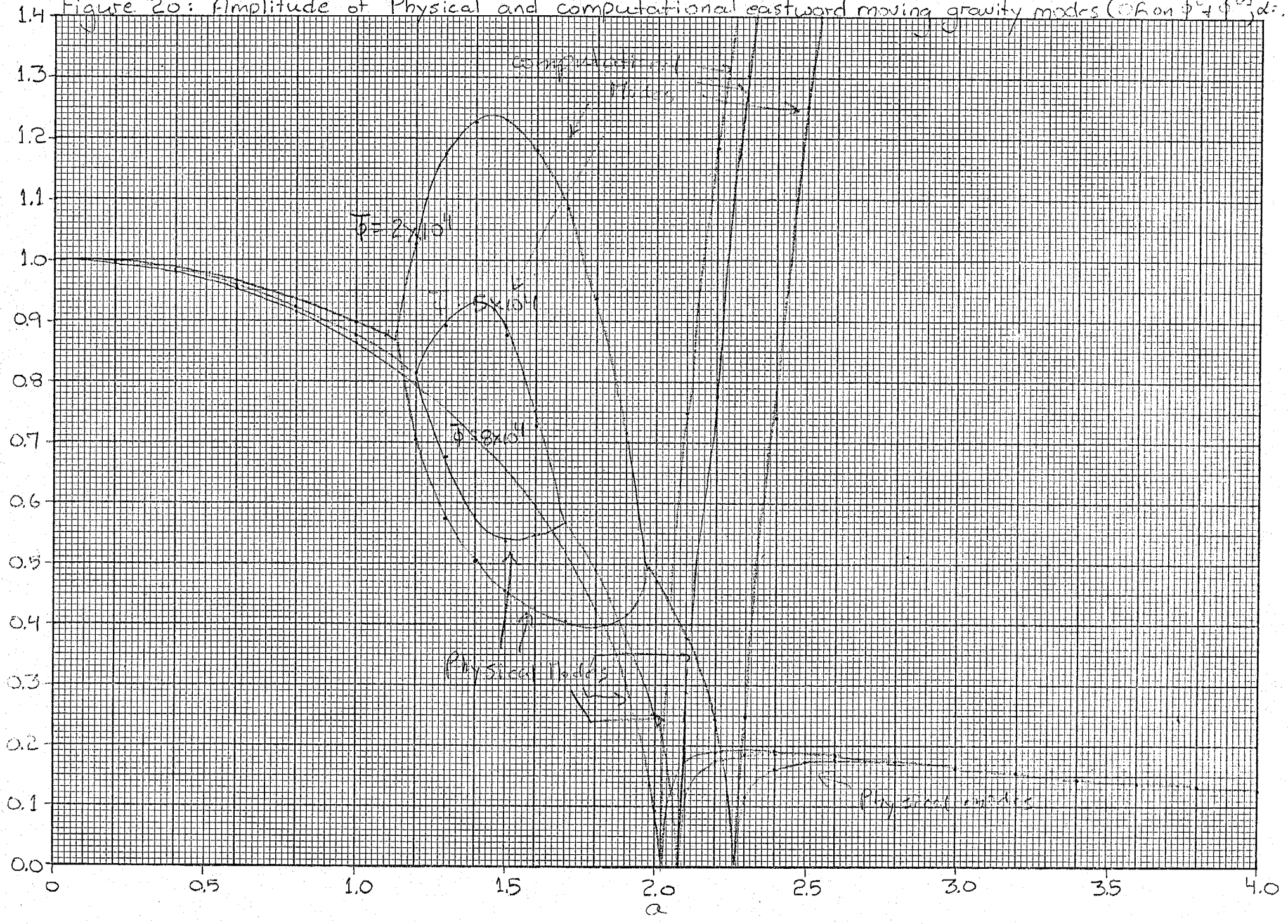

Figure 21: Ratio of Numerical to Analytic Phase Speeds for Physical and Computational Eastward Moving Gravity Modes (OR on ϕ^{τ} and $\phi^{\tau-1}$, $\alpha = .35$)

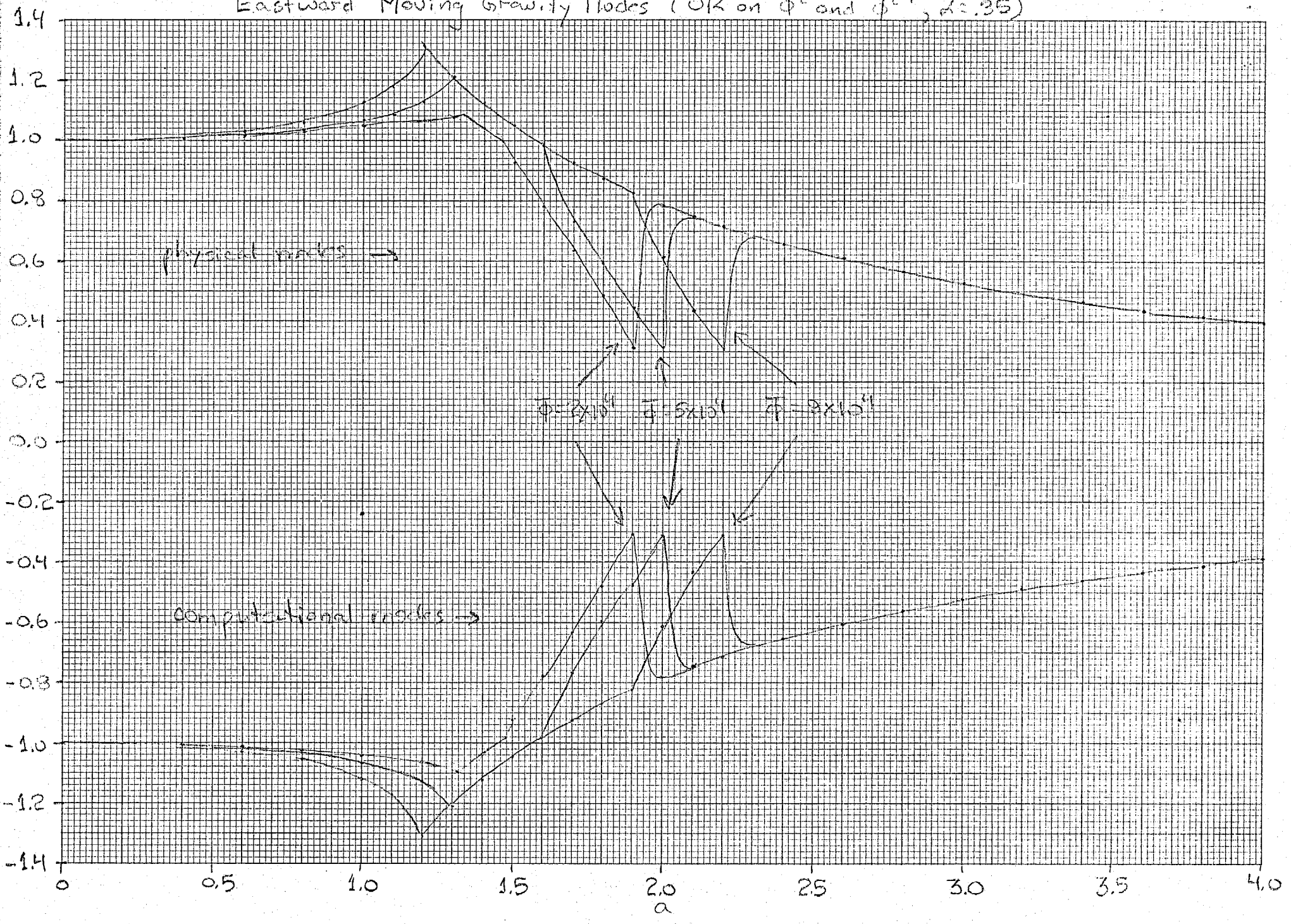

FPI-LOM-20 X 20 TO 1 INCH
5TH, 10TH AND 20TH LINE PROGRESSIVELY ACCENTED

Figure 22: RMS (Divergence) $\times 10^5$ for the 5 forecasts

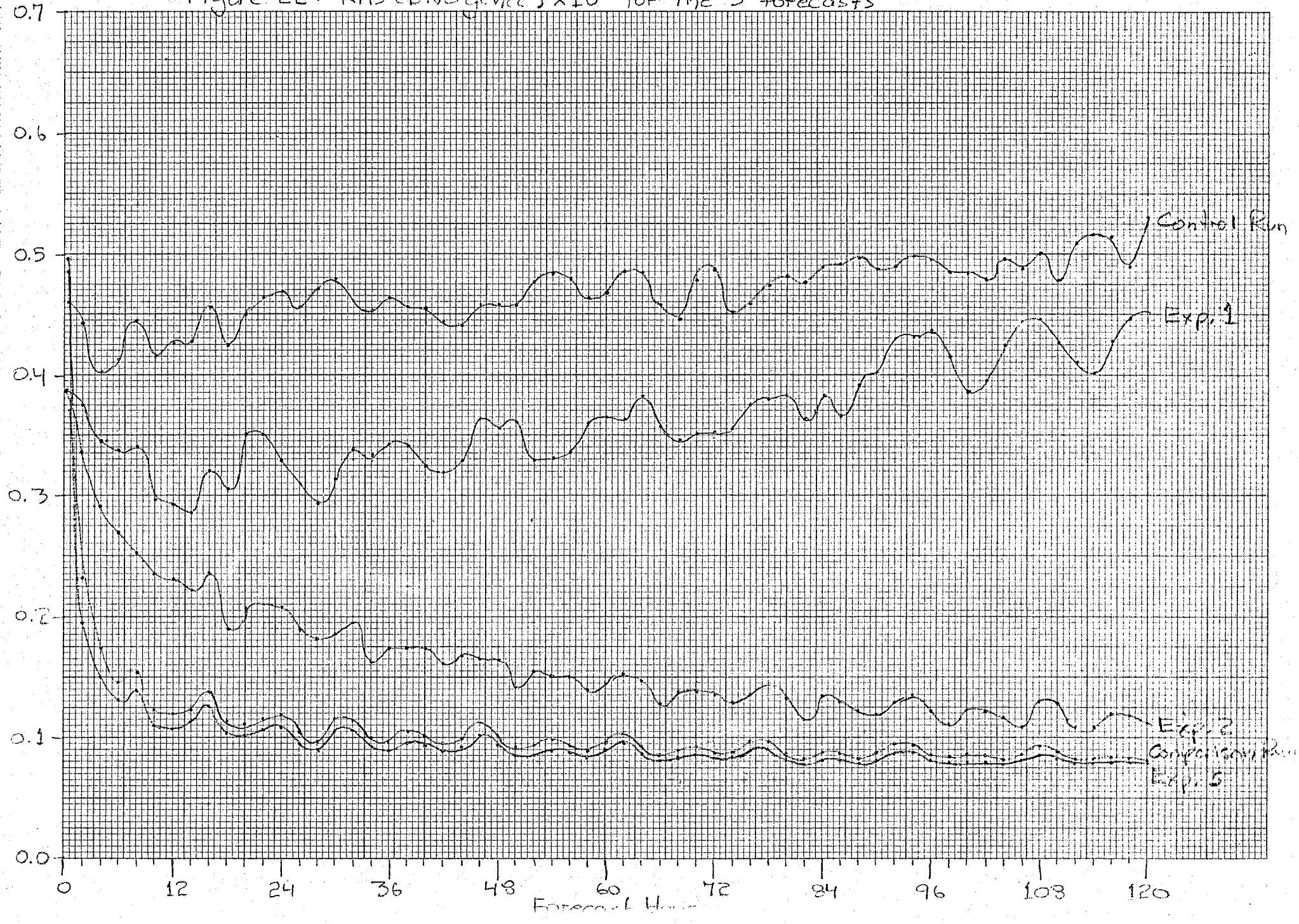

FPI-LOM—20 X 20 TO 1 INCH
5TH, 10TH AND 20TH LINE PROGRESSIVELY ACCENTED

Figure 23: RMS (Vorticity) $\times 10^4$ for the 5 forecasts

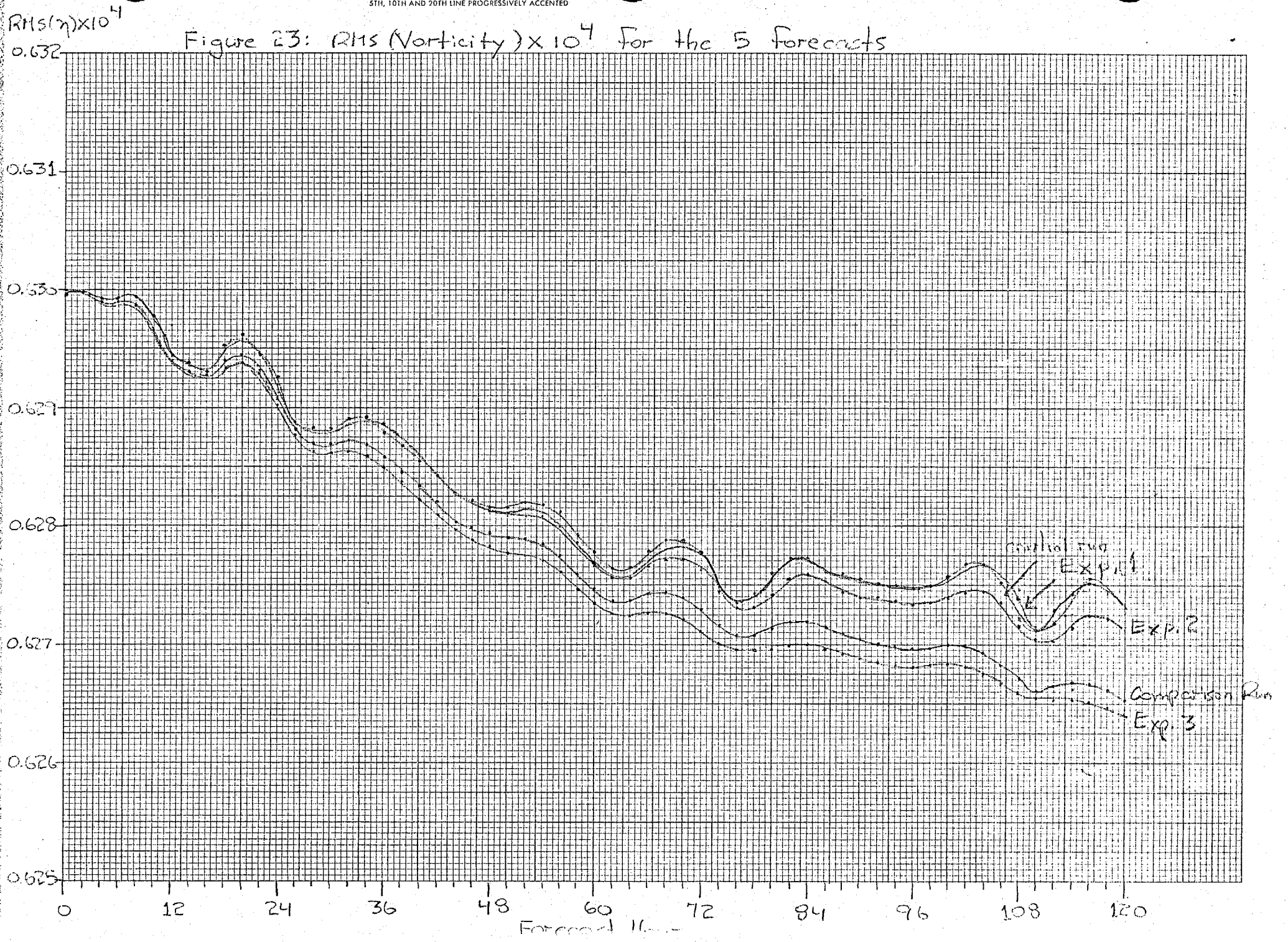

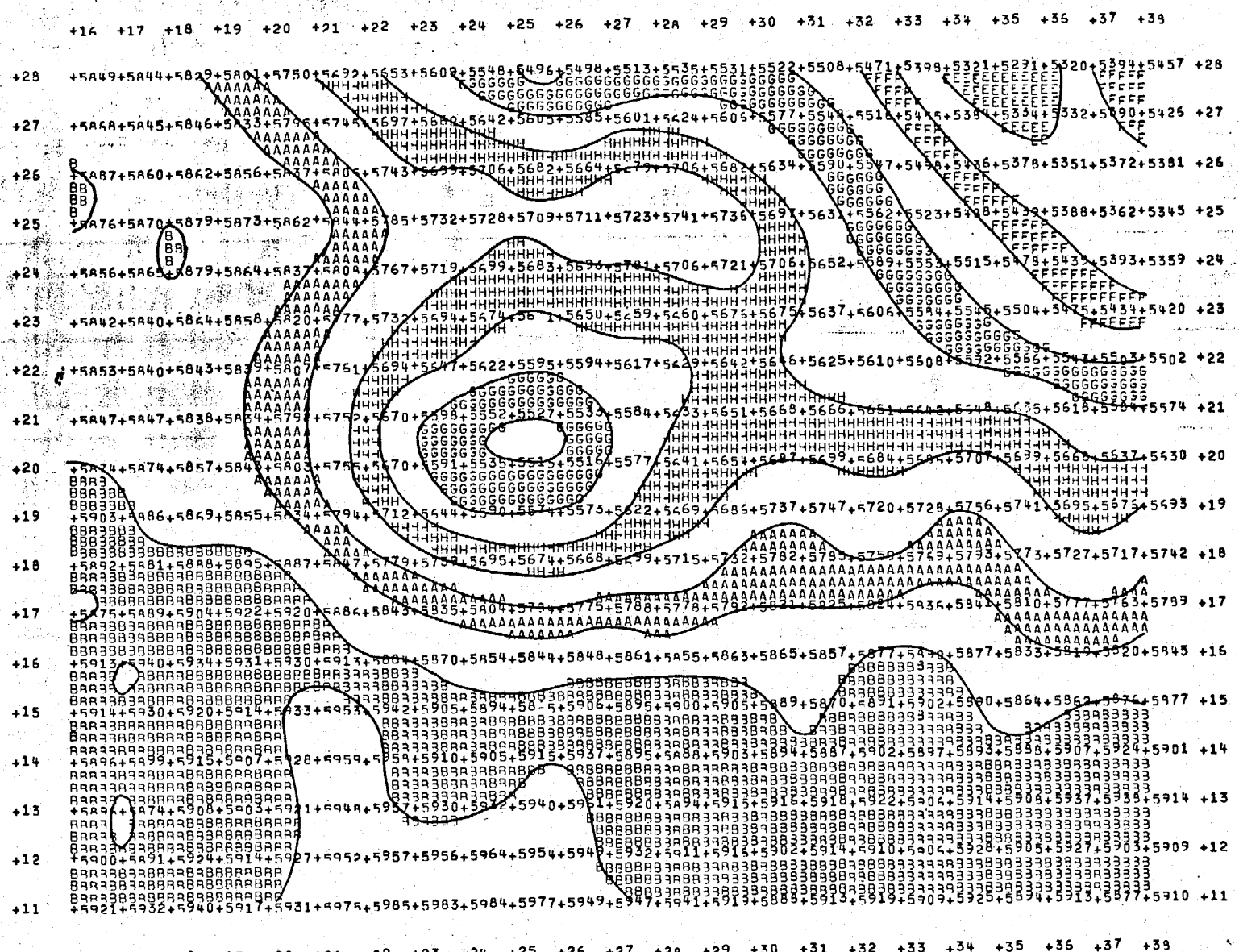

Figure 24: 5-day forecast 500mb Ht. field from the Control Run

HEIGHT

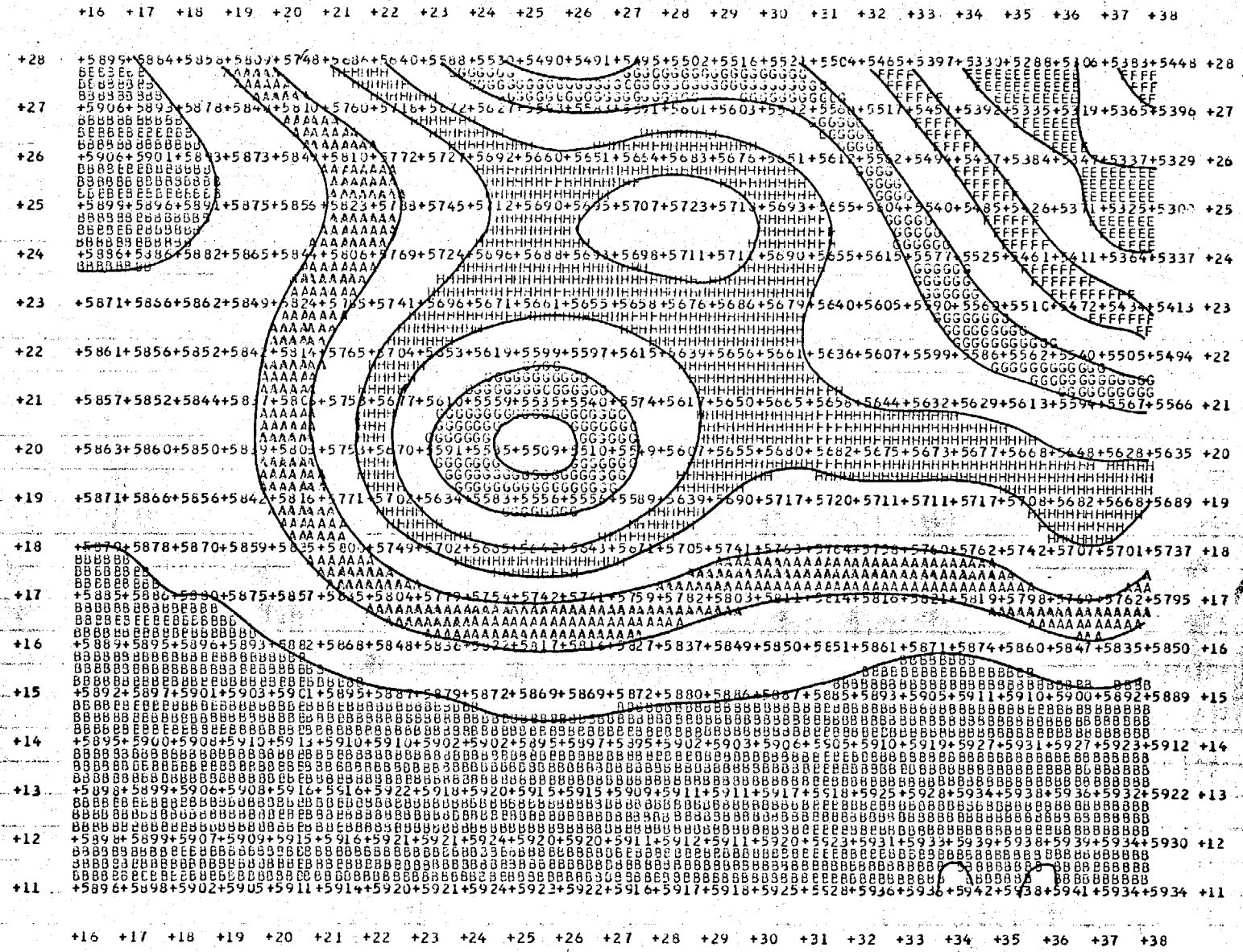

Figure 25: 5-day forecast 500mb Ht. field from the Comparison Run

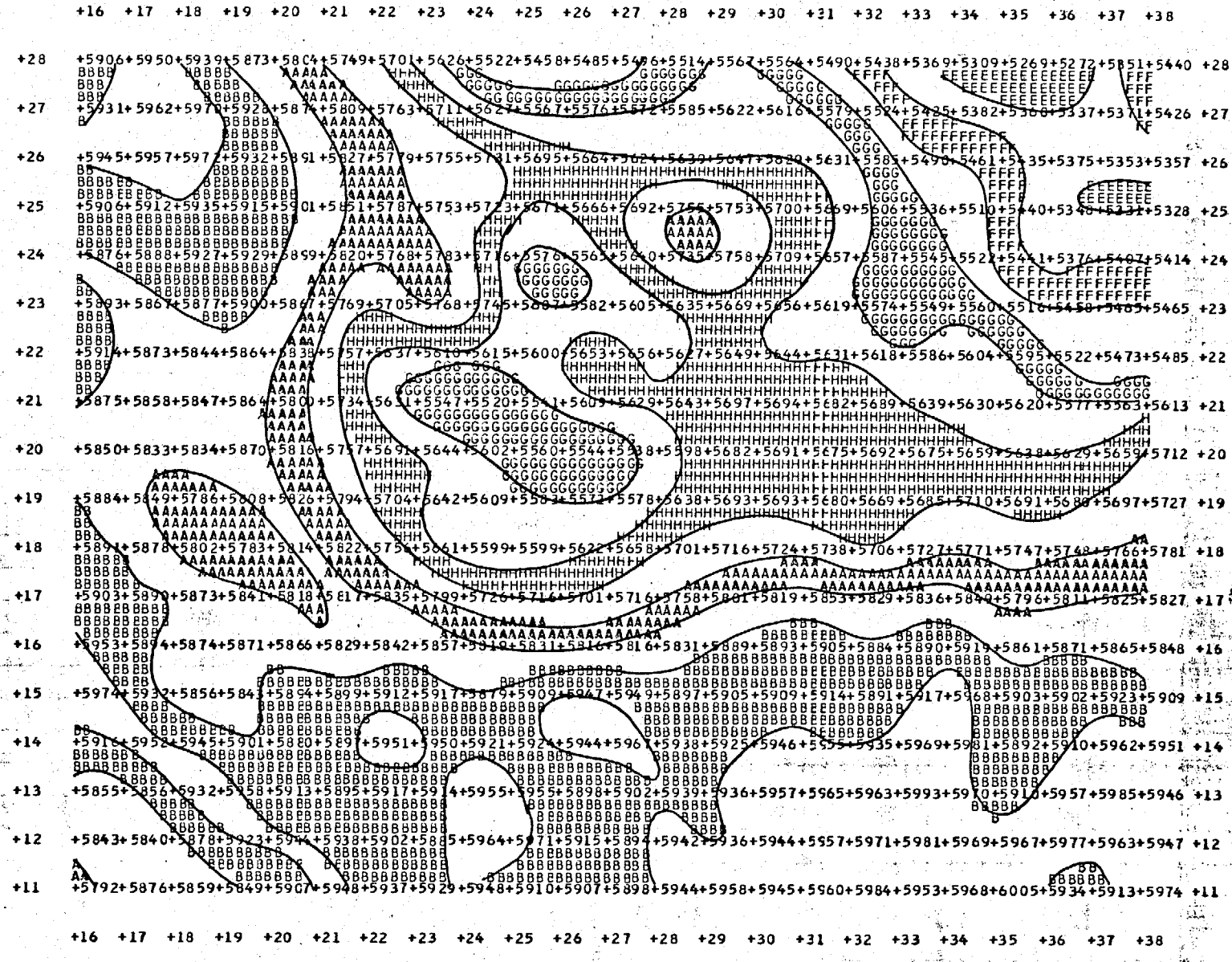

Figure 26: 5 day forecast 500mb ht. field from Exp.1

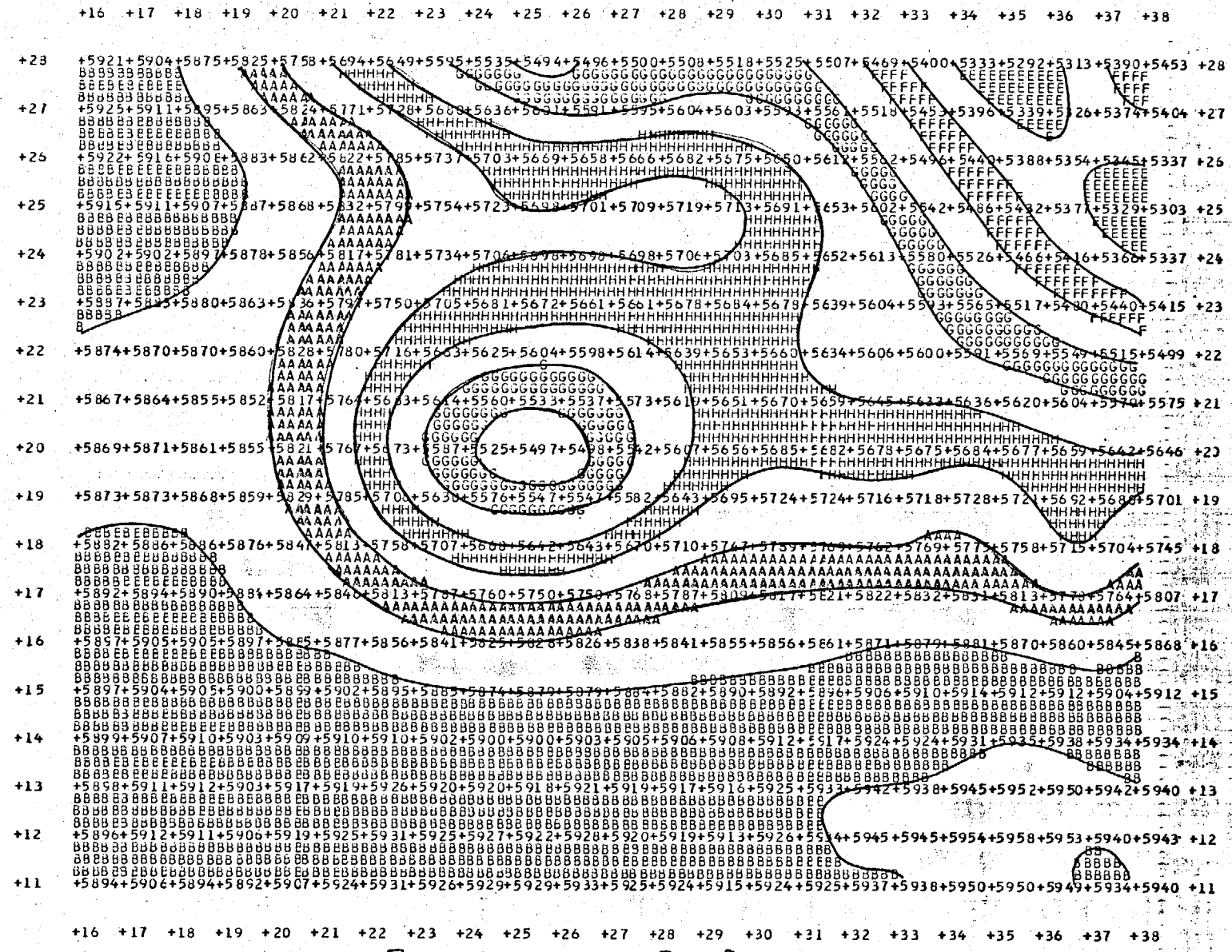

Figure 27: 3-day Forecast 500mb Ht. field from Exp. 2

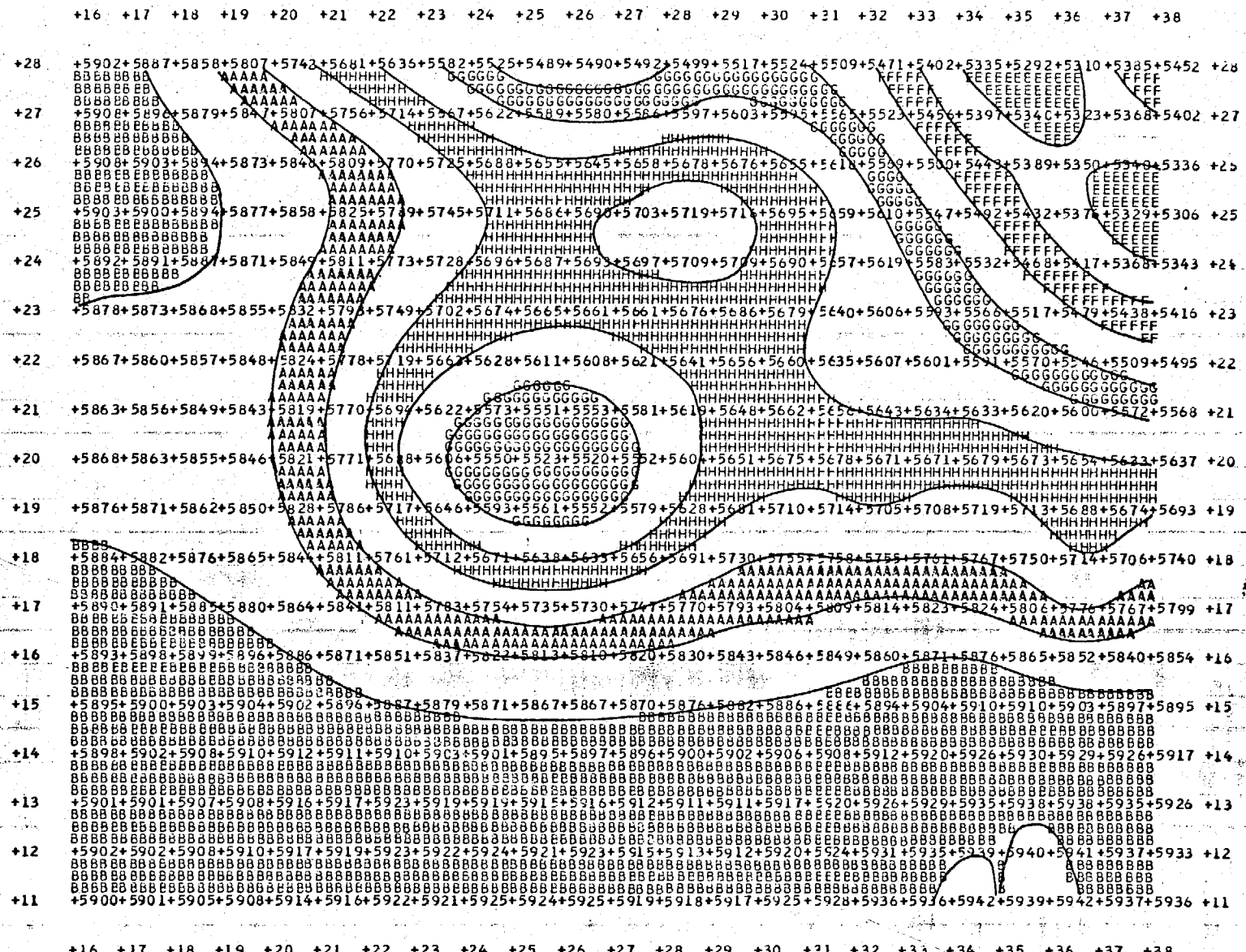

Figure 28: 5-day forecast 500mb Ht. Field from Exp. 3

HEIGHT